



Published in final edited form as:

J Neurosci. 2008 September 24; 28(39): 9769–9789. doi:10.1523/JNEUROSCI.2137-08.2008.

Connexin45-containing neuronal gap junctions in rodent retina also contain connexin36 in both apposing hemiplaques, forming bi-homotypic gap junctions, with scaffolding contributed by zonula occludens-1

Xinbo Li^{1,*}, Naomi Kamasawa^{2,3,*}, Cristina Ciolofan¹, Carl O. Olson¹, Shijun Lu^{1,§}, Kimberly G.V. Davidson³, Thomas Yasumura³, Ryuichi Shigemoto², John E. Rash^{3,4,¶}, and James I. Nagy^{1,#}

¹Department of Physiology, Faculty of Medicine, University of Manitoba, 730 William Avenue, Winnipeg, Manitoba, Canada R3E 3J7

²Division of Cerebral Structure, National Institute for Physiological Sciences, Okazaki 444-8787, Japan

³Department of Biomedical Sciences, Colorado State University, Fort Collins, Colorado 80523, USA

⁴Program in Molecular, Cellular and Integrative Neurosciences, Colorado State University, Fort Collins, Colorado 80523, USA

Abstract

Mammalian retinas contain abundant neuronal gap junctions, particularly in the inner plexiform layer (IPL), where the two principal neuronal connexin proteins are Cx36 and Cx45. Currently undetermined are coupling relationships between these connexins and whether both are expressed together or separately in a neuronal subtype-specific manner. Although Cx45-expressing neurons strongly couple with Cx36-expressing neurons, possibly via heterotypic gap junctions, Cx45 and Cx36 failed to form functional heterotypic channels *in vitro*. We now show that Cx36 and Cx45 co-expressed in Hela cells were co-localized in immunofluorescent puncta between contacting cells, demonstrating targeting/scaffolding competence for both connexins *in vitro*. However, Cx36 and Cx45 expressed separately did not form immunofluorescent puncta containing both connexins, supporting lack of heterotypic coupling competence. In IPL, 87% of Cx45 immunofluorescent puncta were co-localized with Cx36, supporting either widespread heterotypic coupling or bi-homotypic coupling. Ultrastructurally, Cx45 was detected in 9% of IPL gap junction hemiplaques, 90-100% of which also contained Cx36, demonstrating connexin co-expression and co-targeting in virtually all IPL neurons that express Cx45. Moreover, double-replicas revealed both connexins in separate domains mirrored on both sides of matched hemiplaques. With prior evidence that Cx36 interacts with PDZ1 domain of ZO-1, we show that Cx45 interacts with PDZ2 domain of ZO-1, and that Cx36, Cx45 and ZO-1 co-immunoprecipitate, suggesting that ZO-1 provides for co-scaffolding of Cx45 with Cx36. These data document that in Cx45-expressing neurons of IPL, Cx45 is almost always accompanied by Cx36, forming “bi-homotypic” gap junctions, with Cx45 structurally coupling to Cx45 and Cx36 coupling to Cx36.

¶Correspondence regarding FRIL to Dr. John E. Rash, Department of Biomedical Sciences, Colorado State University, Fort Collins, CO 80523, USA. E-mail: john.rash@colostate.edu, #Correspondence regarding immunofluorescence, molecular approaches, and cell culture to Dr. James I. Nagy, Department of Physiology, Faculty of Medicine, University of Manitoba, 730 William Avenue, Winnipeg, Manitoba, Canada R3E 3J7. E-mail: nagyji@ms.umanitoba.ca.

§Present address: Department of Pathology, Weifang Medical College, Weifang Shandong 261042, People's Republic of China

*These authors contributed equally to this work.

Keywords

double-replica; FRIL; heterotypic coupling; homotypic coupling; PDZ domains; SDS-FRL

Introduction

In the retinal inner plexiform layer (IPL), rod and cone pathways are linked to output ganglion cells via abundant gap junctions (Kolb, 1979; Vaney and Weiler, 2000). Of 20 gap junction-forming connexin proteins in the mouse genome (Söhl et al., 2005), mRNA or protein for only two connexins, Cx36 and Cx45, are detected in neurons of mouse IPL (Güldenagel et al., 2000; Feigenspan et al., 2001; Maxeiner et al., 2005). Cx36-containing junctions, in particular, exhibit large-scale ultrastructural diversity (Kamasawa et al., 2006), with different forms correlated with different complements of the gap junction scaffolding and regulatory proteins zonula occludens-1 (ZO-1), ZO-2 and ZONAB (Ciolofan et al., 2006) (ZO-1-associated nucleic acid binding protein; Balda et al., 2003). However, ultrastructural associations of Cx45 with Cx36, morphologies of Cx45-containing gap junctions, and identities of Cx45-associated scaffolding proteins are not established.

Identifying connexins expressed in each neuronal subtype and defining connexin pairing relationships is critical to understanding how, at low light intensity, rod pathways couple via gap junctions to cone bipolar pathways through AII amacrine cell intermediaries (Kolb and Famiglietti, 1974; Vaney and Weiler, 2000; Deans et al., 2002). Initial studies to determine connexin expression patterns employed *in situ* hybridization and single-cell RT-PCR for connexin mRNA detection, or utilized the promoter sequences for Cx45 and Cx36 to drive expression of either lacZ (beta-galactosidase) or enhanced green fluorescent protein (EGFP). The results appeared to demonstrate that many neurons express either Cx36 or Cx45, but co-expression of these connexins was not detected in any retinal neurons (Schubert et al., 2005; Han and Massey, 2005; Söhl et al., 2005; Dedek et al., 2006) except minimally in one study (Lin et al., 2005). Further, Han and Massey (2005) reported that “cx45 immunopuncta never colocalize with cx36 puncta” and suggested that Cx36 and Cx45 form separate populations of homotypic gap junctions. In contrast, Dedek et al. (2006) reported that 30% of Cx45-immunopositive puncta were co-localized with Cx36 and proposed those puncta to represent heterotypic Cx36-to-Cx45 gap junctions, which could account for abundant electrical and tracer coupling of neurons separately expressing Cx36 vs. Cx45 (Maxeiner et al., 2005). That proposal raised difficulties because dye-coupling evidence suggested that Cx36 and Cx45 are unable to form functional heterotypic channels in HeLa cells (Teubner et al., 2000), which led to the suggestion that HeLa cells may lack essential coupling factors that otherwise permit proposed heterotypic coupling of these connexins between IPL neurons (Dedek et al., 2006).

The above discrepancies led us to investigate neuronal gap junctions in rodent IPL according to connexin composition, ultrastructural configurations, and complement of gap junction scaffolding and regulatory proteins ZO-1, ZO-2 and ZONAB. We then analyzed Cx36/Cx45/ZO-1 cellular localization and molecular interactions in HeLa expression systems and in mouse retina using co-immunoprecipitation (co-IP) and pull-down assays. Finally, we used freeze-fracture replica immunogold labeling (FRIL; Rash et al., 2001) and SDS-FRL (Fujimoto, 1995) to co-localize Cx45 and Cx36 in hemiplaques of ultrastructurally-defined gap junctions, including in double-replicas of the same gap junctions. Our results reveal that most if not all Cx45-containing gap junction hemiplaques also contain Cx36, forming Cx36-to-Cx36 plus Cx45-to-Cx45 bi-homotypic gap junctions.

Materials and Methods

Antibodies and animals

Antibodies, their sources and conditions under which they were used in this study are presented in Table 1. Most antibodies were obtained from Invitrogen/Zymed Laboratories (Carlsbad, CA, USA), including a recently available polyclonal antibody generated against a peptide corresponding to a sequence within the c-terminus region of mouse Cx45. Mouse monoclonal anti-Cx45 was also obtained from Chemicon International (now Millipore/Chemicon, Temecula, CA, USA). Specificities of the anti-Cx36, anti-ZO-1, anti-ZO-2 and anti-ZONAB antibodies have been demonstrated elsewhere (Li et al., 2004a; Penes et al., 2005; Ciolofan et al., 2006). Rabbit anti-glutathione S-transferase (GST) Ab06-332 for detection of GST-PDZ domain fusion proteins was obtained from UpState Cell Signaling Solutions (now Millipore, Lake Placid, NY). Monoclonal and polyclonal anti-FLAG antibodies used as control IgGs in co-immunoprecipitation studies were obtained from Sigma-Aldrich Canada (Oakville, Ontario, Canada). For immunocytochemical studies, we used 35 adult male CD1 mice, five male C57BL6/129SvEv wild-type and five Cx36 knockout mice (ko). For FRIL, we used five adult male and five adult female mice [4 albino mice expressing green fluorescent protein (GFP) in locus coeruleus neurons (van den Pol et al., 2002; Rash et al., 2007b) (mice courtesy of Dr. Anthony van den Pol, Yale University), five C57 BL, and one CL3], plus three adult male Sprague Dawley rats. One Wistar rat was used for SDS-FRL double-replicas. All experiments were conducted according to protocols approved by our respective institutional Animal Care Committees, as prescribed in the *Principles of Laboratory Animal Care* (NIH publication No. 86-23, Rev. 1985), with minimization of stress to animals and minimization of the number of animals used.

Light microscope (LM) immunohistochemistry

Mice deeply anesthetized with equithesin (3 ml/kg) under photopic conditions were transcardially perfused with 3 ml of cold 50 mM sodium phosphate buffer, pH 7.4, containing 0.9% NaCl, 0.1 sodium nitrite and 1 unit/ml heparin, and then with 40 ml of cold 0.16 M sodium phosphate buffer, pH 7.6, containing 1% formaldehyde and 0.2% picric acid. To ascertain the extent to which the total exposure to weak formaldehyde alters detectability of connexins, additional mice were perfused with half as much fixative for half the time. In both cases, residual fixative was immediately flushed from animals by perfusion with 10 ml of 25 mM sodium phosphate buffer, pH 7.4, containing 10% sucrose, thereby terminating further formaldehyde exposure. By comparison, other laboratories routinely fix via perfusion with 4% formaldehyde for 10 min (Maxeiner et al., 2005), immersion of Vibratome slices of retina in 4% formaldehyde for 10 min (Güldenagel et al., 2000), or immersion of isolated retinas in 4% formaldehyde for 30 min (Lin et al., 2005). These differences may be important because some investigators detected no Cx45 immunofluorescence in the OFF sublamina of IPL (Güldenagel et al., 2000), whereas other groups detected Cx45 in OFF sublamina and greater density of puncta in ON sublamina (Han and Massey, 2005).

After perfusion fixation, eyes were removed, cryoprotected for 24-72 h in the final rinse, supplemented with sodium azide. Vertical sections of retina were cut (10 μ m) on a cryostat and collected on gelatinized glass slides. Sections were washed for 20 min in 50 mM Tris-HCl, pH 7.4, containing 1.5% sodium chloride (TBS) and 0.3% Triton X-100 (TBSTr). For double immunofluorescence labeling, sections were incubated simultaneously with two primary antibodies for 24 h at 4°C, then washed for 1 h in TBSTr, and incubated for 1.5 h at room temperature simultaneously with appropriate combinations of secondary antibodies, which included: FITC-conjugated horse anti-mouse IgG diluted 1:100 (Vector Laboratories, Burlingame, CA, USA), Cy3-conjugated goat anti-mouse IgG diluted 1:200 (Jackson ImmunoResearch Laboratories, West Grove, PA, USA), Alexa Fluor 488-conjugated goat anti-

rabbit IgG diluted 1:1000 (Molecular Probes, Eugene, Oregon), and Cy3-conjugated donkey anti-rabbit diluted 1:200 (Jackson ImmunoResearch Laboratories). All antibodies were diluted in TBSTr containing 5% normal goat or normal donkey serum. After secondary antibody incubations, sections were washed in TBSTr for 20 min; in 50 mM Tris-HCl buffer, pH 7.4 for 30 min; covered with antifade medium and coverslipped. Some sections single labeled with anti-Cx45 or anti-Cx36 were counterstained with either red Nissl fluorescent NeuroTrace (stain N21482) or green Nissl NeuroTrace (stain N21480) (Molecular Probes). Control procedures included omission of one of the primary antibodies with inclusion of each of the secondary antibodies to establish absence of inappropriate cross-reactions between primary and secondary antibodies or between different combinations of secondary antibodies.

For immunolabeling of HeLa cells grown on poly-L-lysine-treated glass coverslips, cells were fixed with ice-cold 1% or 2% formaldehyde for 5 min, washed in TBS, and incubated for 16 h at 4°C simultaneously with either rabbit anti-Cx45 and mouse anti-ZO-1, or with mouse anti-Cx45 and rabbit anti-Cx43, or with mouse anti-Cx45 and rabbit anti-Cx36 in TBSTr containing normal donkey serum. Cultures were then washed in TBSTr for 1 h and incubated for 1 h at room temperature simultaneously with FITC-conjugated donkey anti-rabbit IgG diluted 1:200 and Cy3-conjugated goat anti-mouse IgG diluted 1:400, or alternatively, with FITC-conjugated horse anti-mouse IgG diluted 1:200 and Cy3-conjugated donkey anti-rabbit IgG diluted 1:400. Slides were washed for 1 h in TBSTr, covered with anti-fade medium and coverslipped.

Conventional and confocal immunofluorescence images were acquired on a Zeiss Axioskop2 fluorescence microscope using Axiovision 3.0 software (Carl Zeiss Canada, Toronto, Ontario, Canada) and on an Olympus Fluoview IX70 confocal microscope using Olympus Fluoview 2.1 software (Olympus Canada Inc., Markham, ON, Canada), and assembled using Adobe Photoshop CS (Adobe Systems, San Jose, CA, USA), CorelDRAW Graphics Suite 12 (Corel Corporation, Ottawa, ON, Canada), and Northern Eclipse software (Empix Imaging, Mississauga, ON, Canada). Some confocal images are presented as z-stacks of five confocal scans at z scanning intervals of 0.4 μ m. However, quantitative analyses of co-localization relationships involving counts of puncta immunopositive for Cx45, Cx36, ZO-1, ZO-2 and ZONAB in vertical sections of the IPL were conducted using single confocal scans with a 60x oil immersion objective lens and a digital zoom magnification of x4 or x5. Counts were obtained from four to ten separate, randomly selected fields along a lateral span of 55 μ m encompassing the inner to outer edge of the IPL in retinas from two to four mice. Values for percentage co-localization were determined for each field and expressed as mean \pm SEM. Numbers of Cx45-positive puncta in the IPL of wild-type and Cx36 ko mice were also determined and evaluated for statistically significant differences using unpaired Student's T test.

For quantitative analysis of the effects of fixation strength and duration on Cx45 co-localization with Cx36, separate data sets were collected from mice perfused with 40 ml of the above described 1% formaldehyde/0.2% picric acid fixative and compared with that obtained from mice perfused with 20 ml of the same fixative, with residual fixative immediately flushed in both cases. Double labeling was conducted using monoclonal anti-Cx45 (Millipore/Chemicon) in combination with either polyclonal anti-Cx36 51-6300 or 36-4600 (Invitrogen/Zymed), or alternatively, using polyclonal anti-Cx45 (Invitrogen/Zymed) with monoclonal anti-Cx36 37-4600 (Invitrogen/Zymed). Because data obtained with these alternative antibody combinations were not significantly different, data were pooled. Since many Cx45-positive puncta (labeled green) in images of IPL were very small, overlay of these images with those of Cx36 (labeled red) were, in cases of Cx45/Cx36 co-localization, often insufficient to produce readily discernible yellow puncta that result from spatial overlap of green and red pixels, hence reducing confidence of establishing degree of co-localization by counting yellow puncta in superimposed images. Instead, quantitative data were acquired by transferring the locations of

green Cx45-puncta onto transparencies and overlaying these transparencies onto images of red puncta representing the more abundant labeling for Cx36.

As a further test for Cx36/Cx45 co-localization in the retina *vs.* simply coincidental overlap of these connexins resulting from the very high density of Cx36 in the IPL, images of Cx36 from the same field double-labeled for Cx45 and Cx36 were flipped horizontally (Han and Massey, 2005) and overlapping Cx45-puncta with Cx36-puncta again counted.

FRIL and SDS-FRL

SDS-FRL (Fujimoto, 1995; Fujimoto, 1997) and FRIL (originally named by Gruijters et al., 1987; as modified in Rash and Yasumura, 1999; Rash et al., 2001) provide for high-resolution immunocytochemical identification of membrane proteins and simultaneous ultrastructural visualization of those proteins in distinctive membrane arrays. SDS detergent, as used in both FRIL and SDS-FRL, does not wash away many cytoplasmic scaffolding proteins that are strongly-bonded to target transmembrane proteins in platinum/carbon-coated replicas, allowing cadherins, catenins, ZO-1, ZO-2, ZONAB, PSD-95 to be immunogold-labeled and localized to tight junctions, gap junctions, adherens junctions and postsynaptic densities (Fujimoto, 1995; Fujimoto et al., 1997; Ciolofan et al., 2006; Kamasawa et al., 2006). We used SDS-FRL for preparation of matched double-replicas (see below) and FRIL for preparation of non-complementary replicas. FRIL combines SDS-FRL with Lexan-stabilization (Steere and Erbe, 1983) and “confocal grid-mapped freeze fracture” (Rash et al., 1995, 1997) for precise histological and ultrastructural mapping of immunogold-labeled gap junctions over square millimeter areas of complex CNS tissues.

For FRIL experiments, both mice and rats were used because previous immunofluorescence studies compared data from both species and reported minor but potentially significant species-specific differences (Feigenspan et al., 2001). In addition, we have published a large FRIL database characterizing distributions and morphologies of >2100 Cx36-containing gap junctions in the IPL of rats and >600 Cx36-containing gap junctions in IPL of mice, establishing the value of both species for comparative ultrastructural and immunocytochemical analyses under a variety of illumination conditions (Kamasawa et al., 2006). Mice and rats were deeply anesthetized with ketamine/xylazine and fixed by transcardiac perfusion with 2% or 4% formaldehyde, as described (Kamasawa et al., 2006). After dissection and collection of Vibratome sections cut at 150- μ m, retina specimens were cryoprotected with 30% glycerol, frozen, freeze-fracture replicated, washed with SDS detergent (Fujimoto, 1995), and immunogold labeled, as described (Rash et al., 2001; Kamasawa et al., 2006).

For FRIL, the same antibodies used for light microscopy (above) were diluted to 10 μ g/ml and applied for 1.2-3 h at either 8°C or 22°C, and secondary antibodies were diluted 1:100 and applied for 11-15 h at either 8°C or 22°C. We have found that this level of dilution, along with an improved “labeling blocking buffer” (Dinchuk et al., 1987) significantly decreases “background”, with only minimal decrease in labeling efficiency, yielding signal-to-noise ratios (SNR) >15,000:1 (Meier et al., 2004). The resulting relatively low labeling efficiency (LE = 1:10 to LE = 1:30, or one gold bead per 10 or 30 connexons) has the dual advantage that gold labels are sufficiently dispersed that they do not resemble “clumps” of gold beads resulting from aggregation of primary or secondary antibodies (Rash and Yasumura, 1999). All commercial antibodies received over the past 10 years and examined electron microscopically immediately upon receipt (>700 different aliquots) had low to moderate numbers and sizes of antibody clumps (data not shown), thereby potentially confounding counts of separate immunogold labels, especially in heavily labeled samples. Regardless, FRIL and SDS-FRL both allow identification of antibody clumps and determination of whether or not clumps occur on ultrastructurally identified gap junctions *vs.* randomly within the neuropil.

To increase immunogold labeling efficiency, thereby potentially increasing detection of one or more connexins in “miniature” gap junctions (*i.e.*, those containing <100 connexons; Rash et al., 2007b), particularly those containing both Cx36 and Cx45, a second set of replicas (Table 3) was labeled for 4.4-5.3 h in primary (*vs.* our normal 1.2-3 h) and for 22 h in secondary antibodies (*vs.* 11-15 h). By way of comparison, previous light microscopic immunocytochemical studies labeled samples with primary antibodies overnight (>10 h) at 4°C (Dedek et al., 2006) or for as long as 3-5 days at 4°C (Lin et al., 2005; Han and Massey, 2005), and for 2-3 h at room temperature (Lin et al., 2005) to overnight at 4°C for secondary antibodies (Han and Massey, 2005; Dedek et al., 2006). Thus, FRIL experiments were at the lower concentration ranges and labeling times normally used for light microscopic and ultrastructural immunocytochemistry. Controls included omission of Cx45 or Cx36 antibodies or substitution of antibodies to some other protein for one or the other connexins. No spurious gap junction labeling was observed in any controls.

Double-replicas by SDS-FRL

For the technically challenging double-replica experiments, one Wistar rat was deeply anesthetized with sodium pentobarbital (50 mg/kg) and fixed by transcardiac perfusion with warmed 2% formaldehyde, 0.85% picric acid in 0.1 M phosphate buffer (pH 7.4). Retinas were removed and embedded in 1% agarose. After collection of Vibratome sections cut at 150- μ m, retina specimens were cryoprotected with 30% glycerol, mounted between 4.6-mm copper sample holders, frozen using an HPM 010 high-pressure freezing device (Bal-Tec/Leica, Wetzlar, Germany), fractured at -105°C in a BAF 060 freeze-fracture machine (Bal-Tec/Leica), sequentially replicated with ca. 2 nm of carbon, 2 nm of platinum, and 20 nm of carbon, and cleaned using 2.5% SDS, 30% sucrose in 15mM Tris-buffered saline (pH 8.3) at 80°C for 18 h (modified from Tanaka et al., 2005; Masugi-Tokita et al., 2007).

For SDS-washed double-replicas, rabbit polyclonal anti-Cx36 antibody (Invitrogen/Zymed) and mouse monoclonal anti-Cx45 antibody (Millipore/Chemicon) were diluted to 5 μ g/ml and applied for 3.5 h at 15°C, and secondary antibody (anti-rabbit IgG 10-nm colloidal gold conjugated, and anti-mouse IgG 5-nm colloidal gold conjugated, both from BBI) were diluted to 1:30 and applied for 24 h at 15°C. After labeling, double-replica samples were photographed using an Olympus SZH dissecting microscope equipped with a CAMEDIA C-3040ZOOM digital camera (Olympus, Tokyo, Japan). Complementary replicas obtained using a hinged double-replica device are mirror images in depth and angle of contour (*i.e.*, hills opposite valleys). To facilitate precise matching of image details, including matching of connexon E-face pits with P-face IMPs in apposed hemiplaques (Challcroft and Bullivant, 1970), one of the complementary replicas was inverted on the specimen support, and the two matching samples were placed in the electron microscope in matching orientations.

Electron microscopy

FRIL replicas were examined at 100 kV with a JEOL 2000 EX-II TEM equipped with a $\pm 60^\circ$ single-tilt stage or a JEOL 1200 EX TEM equipped with a $\pm 45^\circ$ single-tilt stage, and SDS-FRL double-replicas were examined at 80 kV using a JEM 1010 equipped with a $\pm 60^\circ$ single-tilt stage and with a JEOL 2000 EX-II operated at 100 kV. All images were photographed as stereo pairs having an 8° included angle and examined stereoscopically. Digital images (20-80 Mbyte) were obtained from electron microscope negatives using an ArtixScan 2500f digital scanning device (Microtek, Carson, CA, USA) or with an EPSON GT-800 digital scanning device (Seiko Epson, Suwa, Nagano, Japan) and processed using Photoshop CS2 (Adobe Systems). The contrast range for each image was optimized using “levels”. One soft-focus stereopair from the JEOL 1200 (Fig. 9A) was adjusted using “unsharp mask” set with zero “tolerance”. All other images were prepared without unsharp mask. Where appropriate, the contrast ranges over large-areas of some images were digitally “dodged” using “brightness/contrast” functions.

Slight image compressions created by photography of samples tilted for stereoscopy were corrected by using the “image distort” functions and trimmed so that the “stereo windows” appear rectangular and level.

Cx45 expression vector construction

Cx45 cDNA was obtained by reverse transcription of total RNA isolated from adult mouse brain (Li et al., 2004a,b), and the Cx45 coding sequence was amplified using oligonucleotide primers and materials purchased from Gibco BRL Life Technologies (now Invitrogen/Gibco, Burlington, Ontario, Canada). Primers chosen for PCR were designed according to mouse Cx45 sequence (GenBank accession number: NM_008122) and were:

sense primer, 5'-ATGAGTTGGAGCTTCCTGACTCGC-3';

antisense primer: 5'-TTAAATCCAGACGGAGGTCTTCC-3'.

PCR conditions were: initial denaturation at 94°C for 5 min; 35 cycles of amplification with denaturation at 94°C for 60 s, annealing at 52°C for 60 s, and elongation at 72°C for 90 s; and final extension at 72°C for 10 min for T-A cloning. Amplification of Cx45 cDNA by PCR was carried out in 20 µl of solution containing 2 µl of 10 × PCR buffer, 0.8 µl of 50 mM MgCl₂, 200 µM dNTP, 100 ng sense and antisense primers, one unit of *Taq* DNA polymerase and 1 µl of template cDNA. PCR products were separated by electrophoresis in a 1.5% agarose gel prepared using TAE buffer (40 mM Tris-HCl, 0.1% acetic acid, 1 mM EDTA pH 8.0, and 0.0004% ethidium bromide). Separated PCR products were isolated and excised under UV illumination and purified using a gel purification kit (Qiagen Inc, Mississauga, Ontario, Canada). PCR products were subcloned into PCR 2.1 vector, digested with BstX I, and ligated into pcDNA3 expression vector (Invitrogen Life Technologies, Burlington, Ontario, Canada) using T4 DNA ligase (Invitrogen Life Technologies) according to manufacturer's instruction. Cx45 recombinant plasmids were extracted and digested with Xba I to confirm insert orientation and sequenced with M13 forward and reverse primers for sequence confirmation.

Cell culture and HeLa cell transfection

HeLa cells (American Type Culture Collection, Manassas, VA, USA), grown in Dulbecco's Modified Eagle's Medium supplemented with 10% fetal bovine serum and 1% penicillin-streptomycin, were transiently transfected with pcDNA3 vector or Cx45-pcDNA3 plasmids using LipofectAMINE 2000 reagent (Invitrogen Life technologies), as previously described (Li et al., 2004a,b,c). HeLa cells were similarly co-transfected with Cx45 and either full-length Cx36 or truncated Cx36 that lacks the four cterminus amino acids representing the PDZ domain binding motif of Cx36 [prepared as previously described (Li et al., 2004a)]. Transiently transfected HeLa cells were taken for analysis after a 24 h transfection period. For selection of clones stably transfected with Cx45, transfected cells were grown for 24 h and then passaged at 1:40 dilution with fresh Dulbecco's Modified Eagle's Medium containing 1.5 mg/ml of G418, and individual clones expressing Cx45 were isolated after 3 weeks in culture. HeLa cells stably expressing Cx36 were prepared as previously described (Li et al., 2004a). Co-cultures of HeLa cells stably expressing either Cx36, Cx43 or Cx45 (generated as above or provided to us by Dr. K. Willecke, Bonn, Germany) were prepared by mixing equal numbers of Cx43- and Cx45-expressing cells or by mixing equal numbers of Cx36- and Cx45-expressing cells at a density of about 10,000 cells per chamber (1-1.5 cm²) on culture slides for 2 days or until reaching confluence. Transient transfection of Cx45 into HeLa cells stably expressing Cx36 was conducted as described above for transfection of HeLa cells with Cx45.

Western blotting

Deeply anesthetized animals were decapitated, and retinas were dissected, rapidly frozen and stored at -80°C until use. Cx45-transfected and vector-control HeLa cells were rinsed with

PBS buffer (50 mM sodium phosphate buffer, pH 7.4, 0.9% saline), and these cells and retinas were homogenized in IP buffer (20 mM Tris-HCl, pH 8.0, 140 mM NaCl, 1% Triton X-100, 10% glycerol, 1 mM EGTA, 1.5 mM MgCl₂, 1 mM dithiothreitol, 1 mM phenylmethylsulfonyl fluoride and 5 µg/ml each of leupeptin, pepstatin A and aprotinin) and sonicated. Homogenates were centrifuged at 20,000 x g for 5 min, and the supernatants were taken for protein determination using a kit (Bio-Rad Laboratories, Hercules, CA, USA). Western blotting was performed as previously described (Li et al., 2004a,b; Chen et al., 2006). Proteins (50-100 µg of protein per lane from tissue homogenates and 3 µg per lane from culture cell lysates) were separated by SDS-polyacrylamide gel electrophoresis (SDS-PAGE) using either 10% or 12.5% gels followed by transblotting to polyvinylidene difluoride membranes (Bio-Rad Laboratories) in standard Tris-glycine transfer buffer, pH 8.3, containing 0.5% sodium dodecylsulfate (SDS). Membranes were blocked for 2 h at room temperature in TBSTw (10 mM Tris-HCl, pH 8.0, 150 mM NaCl, 0.2% Tween-20) containing 5% non-fat milk powder, rinsed briefly in TBSTw and incubated overnight at 4°C with anti-Cx45 in TBSTw containing 1% non-fat milk powder. Membranes were washed in TBSTw for 40 min, incubated with horseradish peroxidase-conjugated donkey anti-rabbit IgG or anti-mouse IgG diluted 1:3000-1:5000 (Sigma-Aldrich Canada) in TBSTw containing 1% non-fat milk powder, washed in TBST for 40 min and resolved by chemiluminescence (ECL, Amersham PB, Baie d'Urfe, Quebec, Canada).

Immunoprecipitation (IP)

Mouse retinas and HeLa cell lysates were homogenized in IP buffer, sonicated and centrifuged at 20,000 x g for 10 min at 4°C. Following protein determination of sample supernatants, volumes containing 1 mg of protein from mouse retina or from connexin-expressing HeLa cells were pre-cleared for 1 h at 4°C using 20 µl of protein-A-coated agarose beads (Santa Cruz BioTechnology, Santa Cruz, CA, USA), centrifuged at 20,000 x g for 10 min at 4°C, and incubated with either 2 µg of polyclonal anti-ZO-1 antibody, 2 µg of monoclonal anti-Cx45 antibody or 2 µg of polyclonal anti-Cx36 antibody for 16 h at 4°C. The mixture was incubated for 1 h at 4°C with 20 µl of protein-A-coated agarose beads, centrifuged at 20,000 g for 10 min, and the pellet was washed five times with 1 ml of wash buffer (20 mM Tris-HCl pH 8.0, 150 mM NaCl, and 0.5% NP-40). Samples were then mixed with an equal volume of SDS-PAGE loading buffer (125 mM Tris-HCl, pH 6.8, 20% glycerol, 0.3 mM bromophenol blue, 0.14 M SDS, 20% β-mercaptoethanol). For detection of Cx45, samples were boiled for 5 min and taken for immunoblotting with monoclonal anti-Cx45 antibody. For detection of Cx36, samples (not boiled) were immunoblotted with polyclonal anti-Cx36 antibody. Control samples were precipitated with omission of anti-ZO-1, anti-Cx36 or anti-Cx45 antibodies.

GST-PDZ domain of ZO-1 and pull-down assays

Three pGEX-3X plasmids each containing one of the three glutathione-S-transferase (GST)-linked PDZ domains of ZO-1 (Nielsen et al., 2002, 2003) were kindly provided by Dr. B. Giepmans (University of California, San Diego, CA, USA). Preparation of GST-PDZ fusion proteins from these plasmids expressed in *E. Coli* DH5α and binding of fusion proteins to glutathione-agarose beads was conducted as previously described (Li et al., 2004a,b). Beads containing PDZ domain fusion proteins were incubated for 16 h at 4°C with retina that had been homogenized in IP buffer. After extensive washing in PBS buffer containing 1% Triton X-100, proteins from the agarose beads were eluted with SDS-PAGE loading buffer, separated by SDS-PAGE, transferred to blotting membrane and probed with anti-Cx45. After exposure to film, membranes were stripped and re-probed with anti-GST antibody for verifying equal quantities of GST-PDZ domain fusion protein loading.

Results

Distribution of Cx45 and Cx36 in retina

Low magnification images of vertical retinal sections labeled by immunofluorescence and counterstained with Nissl fluorescent NeuroTrace indicate the distributions and relative densities of Cx45 and Cx36 in mouse retina, where immunolabeling consisted exclusively of fluorescent puncta (Fig. 1). Cx45 immunofluorescence was faintly detectable in the OPL (Fig. 1), whereas Cx36 immunofluorescent puncta were substantially more abundant. Both monoclonal anti-Cx45 antibodies from Invitrogen/Zymed and Millipore/Chemicon, as well as polyclonal anti-Cx45 antibody (Fig. 1A) produced punctate labeling throughout the IPL. The polyclonal antibody produced additional sparse but robust labeling at the outer boundary of the inner nuclear layer (INL) (Fig. 1C), as well as punctate labeling along blood vessels in retina (Fig. 1D) and brain (Fig. 1E), consistent with previous descriptions of Cx45 distribution in rodent retina (Dedek et al., 2006) and in cerebral vasculature smooth muscle (Kruger et al., 2000; Li and Simard, 2001). The additional labeling detected with the polyclonal antibody at known tissue locations of Cx45 expression (e.g., blood vessels) suggests that the epitopes of Cx45 on blood vessels are not detected by the anti-Cx45 monoclonal antibodies. Labeling with each of the anti-Cx45 antibodies was observed using optimized fixative containing 1% formaldehyde plus 0.2% picric acid. Greater formaldehyde concentration or greater fixative volume and longer duration of fixation, each followed by washout of residual fixative, substantially suppressed both labeling density and intensity, particularly for very small Cx45-positive puncta, as determined by the lower density of punctate immunolabeling of Cx45 in mice perfused with 40 ml compared with 20 ml of fixative (described below).

In the IPL, Cx36-positive puncta were consistently present at a higher density than Cx45-positive puncta, with the former outnumbering the latter by a ratio of ca. 2:1. Using anti-Cx45 MAB3101 in combination with polyclonal anti-Cx36 antibodies in mice perfused with 20 ml of fixative, counts of puncta yielded 736 ± 27 Cx36-puncta per field and 427 ± 32 Cx45-puncta per field along a $55 \times 55 \mu\text{m}$ X- and Y-axis span of the IPL, with the latter encompassing the full vertical dimensions of the IPL. Labeling for Cx45 compared to Cx36 appears much less than reflected by these numbers due to the much smaller size of Cx45-puncta and the presence of what appeared to be aggregates of Cx36-puncta that could not be separately resolved due to the close proximity of gap junctions in the IPL (Kolb, 1979). This almost certainly led to a vast underestimate of the number of gap junctions containing only Cx36 (Kamasawa, et al., 2006), and here, to underestimates of the ratio of Cx36 to Cx45 puncta. Cx45-puncta were in greater abundance in the inner compared with the outer part of the IPL (Fig. 1A). According to criteria for assigning dimensions of the IPL to inner and outer sublamina (Ghosh et al., 2004) and from counts of Cx45-puncta in confocal images obtained from retinas of mice, the inner three-fifths of the IPL, designated the ON sublamina, contained an average of 297 ± 13 Cx45-puncta along a $55 \mu\text{m}$ X- and Y-axis span of IPL, whereas the outer two-fifths, designated the OFF sublamina, contained an average of 130 ± 31 Cx45 puncta along the same span. Thus, the OFF sublamina has ca. 66% of the volume density of Cx45 puncta as in the ON sublamina. Similar patterns of labeling for Cx45 in the IPL were obtained with polyclonal anti-Cx45. Labeling for Cx36 was densely distributed in the IPL, where it was more concentrated in the inner than the outer half, and moderately concentrated in the outer plexiform layer (OPL) (Fig. 1B). By way of comparison, the density of Cx45 puncta in the OFF sublamina in the briefly fixed samples was higher than in previously published studies, one of which reported an absence of Cx45 in the OFF sublamina (Güldenagel et al., 2000). Specifically, as reported by Dedek et al. (2006) using single confocal scans from mouse retina and using similar objective lenses as used by us, the density of Cx45-puncta in the OFF and ON sublamina of the IPL was 0.0128 and 0.0242 per μm^2 , respectively, whereas we found 0.043 and 0.099 per μm^2 , respectively. The density of Cx36-puncta they reported in the OFF and ON sublamina of the

IPL was 0.0168 and 0.0554 per μm^2 , respectively, whereas we found 0.097 and 0.146 per μm^2 , respectively. These data indicate 3.4-fold to 4.1-fold difference in detection of immunofluorescent puncta for Cx45 in OFF vs. ON layers of IPL and a 5.8-fold to 2.6-fold difference in detection of Cx36. This greater detection of Cx36 cannot be due to non-specific immunolabeling because all immunoreactivity with anti-Cx36 antibodies we used was absent in retina of Cx36 ko mice (described below).

Immunofluorescence co-localization of Cx45 and Cx36 in the IPL

Confocal double-immunofluorescence analysis was undertaken to compare the localization of Cx45 with Cx36 in the IPL (Fig. 2). In general, most puncta immunopositive for the two connexins in the ON sublamina were larger than those in the OFF sublamina, and there appeared to be a decrease in size and density of puncta from the ON to the OFF sublamina (Fig. 2A1, A2). Retinas from twelve mice were examined and similar results were obtained from each. Initial quantitative confocal double-immunofluorescence analyses of Cx45 co-localization with Cx36 was conducted using retinal sections from animals transcardially perfused with 40 ml of fixative. With this fixation protocol, 46% of Cx45-puncta were found to be co-localized with Cx36-puncta (Table 2), approximating the values reported by Dedek et al. (2006). Because this value was substantially lower than the extent of Cx45 co-localization with Cx36 observed by FRIL (described below), we considered the possibility that some labeling of Cx45 was suppressed even with the already weak tissue fixation used (not shown). Thus, quantitative analysis was repeated using retinas from mice perfused with 20 ml of tissue fixative, resulting in a proportional reduction in fixation time because residual fixative in all cases was flushed from animals by perfusion with buffered sucrose. This fixation protocol gave substantially greater numbers of very fine Cx45-puncta (Fig. 2A1) with both polyclonal and monoclonal anti-Cx45 antibodies than were evident with the higher volume and longer duration of fixative. In contrast to the results of Dedek et al. (2006), who found only minor overlap of Cx45 with Cx36 in the OFF sublamina of IPL, our image overlays revealed co-localization of Cx45 with Cx36 in virtually all regions of IPL, and showed that 87% of Cx45-puncta overlapped with Cx36-puncta (Fig. 2A, Table 2). The vast majority of these puncta showed total overlap, rather than partial overlap of adjacent puncta. Conversely, given the greater density of Cx36 than Cx45 in the IPL, most Cx36-puncta were not labeled for Cx45 (not quantified).

Partially overlapping or adjacent puncta were suggested as evidence for heterotypic gap junctions, with Cx36 on one side and Cx45 on the other side (Dedek et al., 2006). However, immunofluorescence labeling for Cx45 and Cx36 in apposing hemiplaques of truly heterotypic gap junctions would precisely overlap and could not be separately resolved by confocal microscopy due to the molecular dimensions of apposed connexons vs. the ca. 0.2 μm limit of resolution of light microscopy. To test whether published images showing “adjacent” puncta for Cx36 and Cx45 are consistent with close association of separate Cx36-homotypic and Cx45 + Cx36 bi-homotypic gap junctions at triadic appositions of cone bipolar cells with AII amacrine cells (see Fig. 29b in Kolb, 1979), and to assess the probability of coincidental association of puncta (Han and Massey, 2005; Dedek et al., 2006), images of Cx36 fluorescent puncta were flipped horizontally in fields double-labeled for Cx45 and Cx36 (Fig. 2B, comparing the same set of images as in Fig. 2A). With the flipped image of Figure 2B2, there was rarely total overlap of individual green and red puncta (Fig. 2B3), as compared with nearly total overlap in non-flipped images. Cx45-positive puncta exhibiting an estimated greater than half area of overlap vs. less than half area overlap with Cx36-positive puncta represented 5.4% ($n = 5$, s.e.m. = 0.4%) vs. 2.8% ($n = 5$, s.e.m. = 0.2%), respectively, compared with 87% co-localization in the non-flipped images. This indicates that Cx45/Cx36 co-localization was not simply a consequence of the high density and large size of Cx36 puncta in the IPL.

To confirm that monoclonal and polyclonal anti-Cx36 antibodies generated against different sequences in Cx36 produced the same level of Cx36 detection, rather than potentially differential levels of labeling, thereby affecting the outcome of Cx36/Cx45 co-localization counts when using these different antibodies, sections were double labeled for Cx36 with monoclonal anti-Cx36 combined with polyclonal anti-Cx36. This combination of two anti-Cx36 antibodies showed nearly total overlap of red and green Cx36-immunopositive puncta (Fig. 2C). Similarly, we tested whether the widely used monoclonal anti-Cx45 antibody from Millipore/Chemicon and the newly generated polyclonal anti-Cx45 antibody recognized the same or partially distinct subsets of Cx45-puncta in the IPL. Double labeling with these antibodies also showed nearly total overlap of immunopositive puncta (Fig. 2D).

FRIL analysis of Cx45 co-localization with Cx36

In samples double labeled for Cx36+Cx45, gap junctions containing Cx45 were found in both OFF and ON sublaminae of the IPL. In addition, a few double-labeled gap junctions were found in the outer plexiform layer (not shown). In 24 FRIL replicas (21 replicas from mice, and 3 from rats) that had been double-labeled for Cx36+Cx45, a large “N” of 671 immunogold-labeled gap junctions were detected (599 in mouse and 73 in rat; Table 3). Of these, 91% (545/599) in mouse IPL and 85% (62/73) in rat IPL were labeled for Cx36 only (Fig. 3A #2), 8% (48/599) and 14% (10/73) in mouse and rat, respectively, were double-labeled for both Cx36 and Cx45 (Figs. 3A1, 3B,C), and 1% (6/599) and 1.4% (1/73) of those in mouse and rat, respectively, were labeled for Cx45 only (Fig. 3D). Approximately 44% (28/64) of Cx45-containing gap junctions were “miniature” gap junctions [*i.e.*, contained <100 connexons; defined in (Rash et al., 2007); see also (Rash et al., 1996)], whereas 50% (32/64) contained between 100 and 400 connexons (0.1-0.2 μm in diameter; defined as “medium-size”), and 6% (4/64) contained between 400 and 2200 connexons (0.2-0.5 μm in diameter; defined as “large”). Overall, 91% (48/53) of Cx45-containing gap junctions in mouse IPL were co-labeled for Cx36. Double-labeled “mini” gap junctions and those larger gap junctions where one or the other connexin is present in low amounts (*i.e.*, <30 connexons) may be difficult to detect by FRIL or by conventional immunofluorescence imaging (Kamasawa et al., 2006), regardless of the overall size of the gap junction, potentially leading to a slight underestimate of co-localization (tested next).

The ratio of the number of gold beads for Cx45:Cx36 within individual Cx45-containing gap junctions varied from 6:1 (*i.e.*, more Cx45) to 1:36 (*i.e.*, much more Cx36), with overall labeling efficiencies (LE) ranging from a LE = 1:3 to LE = 1:59 (*i.e.*, from one gold bead per three connexons to one gold bead per 59 connexons). At the lower LE, some of the few examples of gap junctions containing Cx45 without Cx36 in samples labeled by our standard protocol (<1% of total; 6/671) may represent “false negatives” for Cx36.

As a test for a threshold-of-detection for FRIL based on LE = 1:30 *vs.* LE = 1:10, three replicas were labeled for 5 h in primary antibodies and 21.5 h in secondary antibodies. In these replicas, 156 relatively heavily labeled gap junctions were found, 88% (137/156) of which were labeled for Cx36 only, 12% (19/156) were co-labeled for Cx36+Cx45 (Fig. 3E), and 0% (0/156) were labeled for Cx45 only, suggesting that very nearly 100% of Cx45-containing gap junction plaques also contain Cx36, and that no significant population of gap junctions contained only Cx45 without Cx36. The increased ratio of Cx45-containing to Cx36-containing gap junctions after longer labeling times is not due to increased non-specific labeling because almost all of the largest plaque gap junctions (11/156) and the only large string gap junction encountered (1/156), where non-specific labeling would be most apparent, were labeled only for Cx36 and not for Cx45. Interestingly, in heavily labeled samples (Fig. 3E), the gold beads were concentrated near the periphery of gap junctions, a distribution that is suggestive of steric hindrance of antibody access to the center of larger gap junctions (investigated further, below).

Morphological characteristics of Cx45-containing gap junctions

We previously showed that in IPL, Cx36 was present in a wide variety of morphological classes of gap junctions: designated as crystalline plaques, non-crystalline plaques, reticular, ribbon and string configurations, with string gap junctions associated with more abundant ZO-2 labeling and plaque gap junctions associated with more abundant ZO-1 labeling (Ciolfan et al., 2006; Kamasawa et al., 2006). Ribbon and string configurations represented ca. 50% of Cx36-containing gap junctions in the OFF sublamina. In contrast, almost all (94%; 60/64) Cx45-containing gap junctions in this study were plaques (Fig. 3A-C), several (6%; 4/64) were reticular gap junctions (*i.e.*, plaques with internal voids; Fig. 3D), but none (0%; 0/64) were string or ribbon gap junctions. These differences in morphology suggest that Cx45-containing gap junctions may be associated with different scaffolding proteins than those containing only Cx36 (see below).

Absence of heterotypic Cx36/Cx45 gap junctions in HeLa cells

Teubner et al (2000) reported that in HeLa cells separately expressing Cx36 and Cx45, “None of these co-cultures demonstrated transfer above background of either neurobiotin or Lucifer Yellow (*data not shown*)”, and concluded that Cx45 does not form functional couplings with Cx36. To investigate conditions under which Cx45 and Cx36 engage in gap junction plaque formation together and separately, we used HeLa cells expressing Cx45 and Cx36 to evaluate several potential connexin coupling combinations by immunofluorescence imaging, which was not done in the previous studies. In principal, a connexon hemichannel may assemble from six identical connexin monomers to form “homomeric” connexons (Fig. 4A-F) or assemble from two or more different connexins to form “heteromeric” connexons (Fig. 4G,H). In turn, connexons may link to identical homomeric connexons to form “homotypic” channels (Fig. 4A,B,E), or they may link to connexons containing unlike connexins to form “heterotypic” channels (Fig. 4C,D). Because FRIL revealed that Cx45 was almost always accompanied by Cx36 within individual hemiplaques in retina (supporting either 4E, 4F, 4G or 4H), we tested whether homomeric Cx45 hemichannels can form heterotypic plaques by coupling with homomeric Cx36 hemichannels (as in Fig. 4C). First, as a positive control for the ability of HeLa cells to form homomeric heterotypic junctional plaques consisting of Cx45-to-Cx43 channels (as in Fig. 4D), HeLa cells expressing Cx45 (Cx45-HeLa) were co-cultured with cells stably expressing Cx43 (Cx43-HeLa). In mixtures of these cells grown to near confluence, double immunofluorescence labeling showed that within colonies of cells expressing either one or the other connexin, they formed either Cx45-positive plaques (Fig. 5A1) or Cx43-positive plaques (Fig. 5A2) at apposing cell membranes. At locations where Cx45 colonies abutted Cx43 colonies, Cx45-immunofluorescent puncta at cell appositions were co-localized with Cx43 (Fig. 5A3), suggesting that these connexins form homomeric heterotypic gap junctions (as in Fig. 4D), consistent with the permissiveness of these connexins to form functional gap junctions (Elfgang et al., 1995; Rackauskas et al., 2007). Second, in mixtures of HeLa cells stably expressing only Cx36 (Cx36-HeLa) co-cultured with cells stably expressing only Cx45, colonies of cells expressing either Cx45 or Cx36 were found to display large numbers of Cx45-puncta (Fig. 5B1) or Cx36-puncta (Fig. 5B2) within their respective colony compartments. At abutments of these homotypically-expressing cells, there was a total absence of Cx45/Cx36 co-localization (Fig. 5B3), and this was consistent throughout the co-culture, indicating failure of gap junction plaque formation between Cx45-HeLa and Cx36-HeLa cells. This shows that in HeLa cells, homomeric Cx36 does not form heterotypic channels with homomeric Cx45 (*i.e.*, inability to form configuration shown in Fig. 4C). Similar results were obtained whether we used Cx45-HeLa cells provided to us by K. Willecke (Bonn, Germany) or those generated as described in MATERIALS AND METHODS. Based on the ability of Cx45- and Cx43-expressing HeLa cells to form heterotypic gap junctions (Fig. 5A3), this failure to form heterotypic Cx36-to-Cx45 gap junctions in the same cells that separately form homotypic gap junctions cannot be due to an internal deficiency of connexin sorting,

transport or connexin interaction with scaffolding proteins. Consequently, the possibility of Cx45/Cx36 heterotypic coupling was investigated further.

After transient transfection of Cx36-HeLa cells with Cx45, adjacent pairs of cells expressing both of these connexins displayed Cx45/Cx36 co-localization at points of plasma membrane apposition (Fig. 5C), indicating the ability of HeLa cells to traffic the co-expressed connexins to common membrane locations, apparently to the same gap junctional plaques, as occurs in retina. Also encountered were pairs of adjacent Cx36-HeLa cells that were each transiently transfected with Cx45 and that formed Cx36/Cx45 co-localized plaques at points of contact with each other; however, where Cx45/Cx36 cells contacted adjacent cells expressing only Cx36, they displayed only Cx36-containing plaques (Fig. 5D). This shows that Cx45 connexons do not simply undergo co-trafficking with Cx36 connexons to plasma membranes, but rather require Cx45-containing connexons in the adjacent cell to achieve stable plasma membrane localization. These observations also indicate that Cx45 co-expressed with Cx36 does not form heteromeric connexons in one cell that couple with homomeric Cx36 connexons in the other cell, but that when Cx45 is co-expressed in Cx36-expressing HeLa cells, they form bi-homotypic plaques (*i.e.*, as in Fig. 4E). However, because neither single-replica FRIL nor immunofluorescence imaging have sufficient resolving power, these experiments do not eliminate the possibility that Cx36 and Cx45 may form individual heteromeric connexons that stably couple to either heteromeric or homomeric connexons in apposing cells (as in Figs. 4G, 4H), but this is considered unlikely because Cx36 and Cx45 are in different connexin classes (Söhl and Willecke, 2003) that are proposed to be incapable of forming heteromeric connexons (Evans and Martin, 2002). Nevertheless, the arrangement of homomeric *vs.* heteromeric connexons might be ascertained by double-replica FRIL if labeling for the two connexins were to be unequivocally segregated (examined in next section).

Double-replica analysis of Cx45 and Cx36 in apposed hemiplaques in rat IPL

Because conventional FRIL is based on random fracturing through complex tissue, a sufficiently large sample size will reveal all possible configurations of gap junctions and accurately reveal the range of connexon labeling and connexin pairing relationships. The absence of a significant population of gap junction plaques containing only Cx45 (0.6%, all data combined) means that there is no significant population of gap junctions containing only Cx45 in only one hemiplaque or in both apposed hemiplaques. Only by the use of double-replicas showing both sides of the same gap junction could it be proven that both connexins are contained in both sides of a pair of hemiplaques. Moreover, the above immunofluorescence results documenting gap junction plaque-forming capability of Cx45 and Cx36 in HeLa cell expression systems underscored the necessity for examining matched double-replicas of Cx45-containing gap junctions in retina.

In both single and double-replicas the fracture plane always separates apposed connexons at their point of contact in the extracellular space (Fig. 6A, as previously shown, Fujimoto, 1997; Rash and Yasumura, 1999; Nagy et al., 2004), separating gap junctions into two complementary hemiplaques, each containing connexons from only one or the other cell (Fig. 6B,C). Immunogold labeling of cytoplasmic epitopes of connexons occurs in the residual cytoplasm beneath the Pt/C replica (Fig. 6B,C). Moreover, labeling is approximately equal beneath both E-face pits and P-face particles, demonstrating that the connexons of the subjacent cell are retained and not washed away during SDS cleaning (Fujimoto, 1997; Rash and Yasumura, 1999). In the case of double-replicas, however, both fracture faces are retained and replicated, and both sides are approximately equally well labeled in the matching complementary images of both E-face pits and P-face IMPs (Figs. 6B-C and 6D-G). This feature for clean separation of hemiplaques in vertebrate gap junctions allows definitive assignment of one or multiple connexins to individual hemiplaques belonging to one or the

other apposed cell (Rash et al., 2001,2004;Nagy et al., 2004;Kamasawa et al., 2005), and equally important, potentially allows assessment of whether Cx45 and Cx36 are intermixed (as heteromeric connexons, Fig. 4G,H) or segregated into domains of homomeric connexons (Fig. 4E).

In double-replicas of complex neuropil, multiple structural markers are used to find the same gap junction in both complementary replicas. However, corresponding areas in one or the other replica are often missing because: a) one or the other may be covered by grid bars, even when using thin-bar slot grids (Fig. 6D,D'; dotted lines on each sample correspond to locations of obscuring grid bars in the complementary replica); b) fragmentation and loss of complementary areas may occur during sample processing (Fig. 6D,D'; outlines indicate portions lost in its complementary replica); or c) one or the other matching area was obscured by adhering debris (one example, not shown). Nevertheless, in a large portion of one set of matched double-replicas (Fig. 6D,D'), we found >160 immunogold-labeled gap junctions, including 11 Cx45-containing gap junctions that had matching complements, five of which are illustrated here (Figs. 6, 7, and Supplementary Fig. S1). Eight of these 11 pairs were labeled for both Cx45 and Cx36 in both matching hemiplaques. In these matched pairs, the number of gold beads for the two connexins were substantially greater in one vs. the other hemiplaque in six pairs (Fig. 6F,G and Supplementary Fig. S1A), and approximately equal in two paired hemiplaques (Fig. 7). In six of eight pairs, Cx45 and Cx36 appeared to be segregated into domains, with labels for both connexins beneath their respective complementary sectors in the mirror hemiplaques (*i.e.*, Cx45 opposite Cx45 and Cx36 opposite Cx36; Fig. 6F-G and Fig. 7). This observed segregation of labels implies that the connexons are present in homomeric connexons that are further segregated into domains containing either Cx36 or Cx45 but not both (*i.e.*, correspond to Fig. 4E but not to 4G or 4H). Variations in number of labels for each connexin in matched pairs are attributed to stochastic differences arising from the numerically low labeling efficiency (LE = 1:15 to 1:20) in these matched pairs vs. the relatively few connexons of each connexin type, particularly in smaller gap junctions. Minor discrepancies in positions of gold beads (Fig. 6G, arrows) are attributed to the 28-nm “radius of uncertainty” of immunogold labeling (Fig. 6B,C) or to the displacement of connexons into lipid “blebs” formed during SDS washing (Rash and Yasumura, 1999; Kamasawa et al., 2006). These few examples of apparent segregation of each connexin into discrete domains do not eliminate the possibility that homomeric homotypic Cx45- and Cx36-connexons may also be intermixed in some gap junctions. However, the relatively low labeling efficiency could not preclude the existence of a few heteromeric connexons. Nevertheless, our immunocytochemical data showing absence of Cx45/Cx36 heterotypic coupling (Fig. 5), plus FRIL data in which 60 of 64 (and 19/19; see Table 3) Cx45-labeled gap junctions also contained Cx36, combined with data from six of eight mirrored gap junctions showing approximate alignment of Cx45- vs. Cx36-containing domains, unequivocally document that Cx45 and Cx36 are present, together on both sides of the same gap junction, presumably with homomeric Cx45 connexons coupling with homomeric Cx45 connexons, and homomeric Cx36 connexons coupling with homomeric Cx36 connexons. This bi-homotypic coupling pattern occurred in most if not all Cx45-containing gap junctions in mouse and rat IPL.

In three of the eight mirror pairs from the ON sublamina of IPL, double-labeled gap junctions were adjacent to linear arrays of postsynaptic E-face particles characteristic of ribbon synapses (Fig. 7, inscribed box), which in IPL, occur only in cells postsynaptic to rod and cone bipolar cells (Kolb, 1979). In each of these three mirror pairs, the cell that was postsynaptic to the ribbon synapse was linked to an unidentified third cell by a gap junction containing both Cx45 and Cx36 in both sides (inscribed ovals). Thus, these coupled cell pairs that were postsynaptic to bipolar cells in the ON sublamina co-expressed and co-targeted Cx45 and Cx36.

Of the remaining three gap junction pairs with unequal labeling of apposed hemiplaques (from 11 total), one small gap junction (37 connexons) was labeled for both Cx36 (seven gold beads) and Cx45 (two gold beads) on one side but was not labeled for either connexin on its matched complement (not shown). Assuming that the gap junction contained no more than about 10 Cx45 connexons and 27 Cx36 connexons, and a nominal LE = 1:20, the complete absence of labeling for either connexin on the unlabeled side would be consistent with normal stochastic variability of labeling. The second asymmetrically labeled gap junction (ca. 100 connexons) had three gold beads for Cx45 and 7 gold beads for Cx36 on one side and zero gold beads for Cx45 and five gold beads for Cx36 on the complementary surface. The third of three unequally-labeled pairs was a large gap junction (>400 connexons) that was well labeled for Cx36 in both the upper and lower hemiplaques (37 and 32 gold beads, respectively; supplementary Fig. S1B) but contained only a single gold bead for Cx45 on one side and none on the other side. The latter pair of images could imply that there were equally few Cx45 connexons in the mirror hemiplaque, or it could imply the presence of a few unpaired Cx45 connexons. However, this discrepancy of one vs. zero gold beads for Cx45 is also consistent with normal stochastic differences in connexin labeling efficiency.

Statistical analysis of Cx45 relationships with Cx36 in retinal neurons and gap junctions

To test various hypotheses regarding expression and localization of Cx36 and Cx45 in the retina, we used a web-based online statistical analysis system to calculate confidence intervals (<http://www.measuringusability.com/wald.htm>) (see Hypothesis 3, below).

Hypothesis 1: Cx45 and Cx36 are separately expressed in a neuron subtype-specific manner—The hypothesis that Cx45 is not co-expressed in cells that express Cx36 is nullified by finding in single replicas that most (60 of 64) Cx45-containing gap junctions also had Cx36 labeling (Table 3), and further nullified by 19 of 22 mirror hemiplaques in double-replicas showing that both connexins occur in the same cell (Figs. 6,7). However, the four of 64 examples of Cx45 labeling without Cx36 labeling are consistent with either: a) incomplete (*i.e.*, false negative) labeling for Cx36 in a very small fraction (4/64) of Cx45 expressing cells, b) lack of simultaneous insertion of Cx36 with Cx45 into plaques (whereas endocytotic retrieval of connexons involves internalization of structurally-coupled membrane patches; Gaietta et al., 2002), or c) existence of a small fraction of Cx45-expressing cells that do not co-express Cx36. In the latter case, Hypothesis 1 might still apply, but at most, only to a very small fraction of Cx45-expressing cells.

Hypothesis 2: Cx45-expressing cells have hemiplaques containing only Cx45, either as mono-homotypic (Cx45-to-Cx45) or heterotypic (Cx45-to-Cx36;) gap junctions—Hypothesis 2 is invalidated by the demonstration in single replicas that >90% (60/64) of Cx45-containing hemiplaques also contain Cx36 (Fig. 3 and Table 3). Similarly, double-replicas showed that none of 11 matched pairs of Cx45-containing gap junctions had only Cx45 in either of their apposed hemiplaques (Figs. 6,7, and S1), further invalidating Hypothesis 2.

Hypothesis 3: Cx36 is present in Cx45-containing gap junctions, forming bi-homotypic plaques—Table 4 presents the percentages, along with 95% confidence intervals (CI), for Cx45+Cx36 forming bi-homotypic gap junctions in mouse and rat IPL in both single-replicas and double-replicas, where 93.8% to 100% of Cx45-containing gap junctions also contain Cx36. Moreover, eight of 11 pairs of Cx45-containing gap junctions found in double-replicas contained both Cx45 and Cx36 in both sides, with six of those pairs, to the limit of the radius of uncertainty of immunogold labeling, having near precise mirror distributions of labels for both connexins, thereby demonstrating the presence of bi-homotypic gap junctions that also are primarily or exclusively homomeric.

Cx45 in relation to ZO-1, ZO-2 and ZONAB in retina

To further characterize the basis for Cx45 occurrence almost exclusively in plaque but not string gap junctions, we investigated possible differences in their co-associated cytoplasmic scaffolding and accessory proteins. We previously documented a high degree of co-localization of Cx36 with the cytoplasmic proteins ZO-1, ZO-2 and ZONAB in plaque, reticular, ribbon and string gap junctions in mouse retina, as well as direct molecular interaction of Cx36 with ZO-1 (Li et al., 2004a; Ciolofan et al., 2006). Based on evidence provided above for Cx36 in most Cx45-containing plaque gap junctions, confocal double-immunofluorescence analysis was undertaken to determine whether Cx45/Cx36 junctions are associated with each of the above accessory proteins or whether they represent a distinct subpopulation of Cx36-containing junctions lacking one or more of these scaffolding proteins. In vertical scans of retina presented as z-stack images of five scans, Cx45 was substantially co-localized with ZO-1 (Fig. 8A), as seen by presence of yellow puncta resulting from green/red overlap. From counts of puncta in IPL of retinal sections that were double-immunolabeled for Cx45 and ZO-1, conducted using single confocal scans to avoid puncta overlap in the z-axis, 71% of Cx45-puncta were found to be co-labeled and to exhibit total overlap with ZO-1 (Table 2). However, the vast majority of ZO-1-puncta were localized at structures other than Cx36- and Cx45-containing gap junctions, including adherens junctions of the outer limiting membrane (Ciolofan et al., 2006). After horizontal flipping of the ZO-1 image to form new overlay images (Fig. 8B), Cx45-positive puncta exhibiting an estimated greater than half area of overlap vs. less than half area overlap with ZO-1-positive puncta represented 11% (n = 5, s.e.m. = 2%) vs. 6.4% (n = 5, s.e.m. = 0.5%), respectively, as compared with 71% in unflipped images. As observed for Cx45, the labeling density for ZO-2 was sparse, and little Cx45/ZO-2 co-localization was observed (7%, Table 2) in all fields examined (Fig. 8C). Similarly, double labeling and counts of puncta in single confocal scans indicated negligible Cx45-puncta overlap with ZONAB-puncta (Table 2, and Fig. 8D). In contrast, 39% of Cx36-positive puncta contained ZONAB, as previously described (Ciolofan et al., 2006). Thus, ZO-1 but not ZO-2 or ZONAB are present in and characteristic of Cx45-immunopositive puncta.

Cx45 and ZO-1 in retina of Cx36 ko mice

The presence of ZO-1 at gap junctions containing Cx45 suggested its association either with Cx45 or exclusively with Cx36 that is also contained in most of these junctions and with which ZO-1 was recently found to be highly co-localized (Li et al., 2004a). This question was addressed by comparing labeling patterns of Cx45 in retina of wild-type and Cx36 ko mice. Double immunofluorescence labeling was conducted to determine whether the presence of Cx36 at Cx36/Cx45 co-localized puncta was required for Cx45/ZO-1 association. As shown by image overlay (Fig. 8E), substantial Cx45/ZO-1 overlap was found in Cx36 ko mice. Counts of puncta revealed that $78 \pm 4.2\%$ and $78 \pm 2.4\%$ of Cx45-puncta were co-localized with ZO-1 in the IPL of retina from wild-type and Cx36 ko mice, respectively, which indicated that elimination of Cx36 had little effect on Cx45/ZO-1 association and suggested direct molecular interaction of Cx45 with ZO-1, as examined further, below. Confocal double immunofluorescence in vertical sections of retina from wild-type C57BL/6 mice indicated similar labeling and distribution of Cx36 and Cx45 in the IPL (Fig. 8F,G) as observed in CD1 mice (Figs. 1 and 2). Double immunofluorescence imaging in retina of Cx36 ko mice showed an absence of labeling for Cx36 in the IPL (Fig. 8H) and reduced labeling of Cx45 (Fig. 8I). Counts of Cx45-puncta in eight randomly selected fields in the IPL from wild-type and Cx36 ko mice revealed a significant 25% reduction ($p < 0.05$) of Cx45-puncta in the ko mice.

FRIL analysis of Cx45 co-localization with ZO-1

SDS digestion (as used in SDS-FRL and FRIL) does not separate transmembrane proteins from many of their tightly-bound cytoplasmic scaffolding and accessory proteins, leaving many of

those molecules available for detection by immunogold labeling (Fujimoto, 1997; Fujimoto et al., 1997; Ciolofan et al., 2006). In a replica that was double labeled for Cx45 (Millipore/Chemicon monoclonal antibody) plus ZO-1 (Invitrogen/Zymed rabbit polyclonal antibody), 48 labeled gap junctions were found (Fig. 9). Of these, 44% (21/48) were double-labeled for Cx45 plus ZO-1 (Fig. 9A,B), 4% (2/48) were labeled for Cx45 only (not shown), and 52% (25/48) were labeled for ZO-1 only (Fig. 9C,D), including five string gap junctions (Fig. 9C). In this replica, which was labeled relatively briefly (1.25 h in primary antibodies and 16 h in secondary antibodies), 91% (21/23) of Cx45-labeled gap junctions were co-labeled for ZO-1. This means that ZO-1 is on both sides of most, if not all, Cx45-containing gap junctions. The remaining 25 gap junctions (52%) were labeled for ZO-1 without Cx45, consistent with observations from immunofluorescence labeling (see above) and from FRIL (Kamasawa et al., 2006; Ciolofan et al., 2006) that many from the larger pool of homotypic Cx36-containing gap junctions also have closely bound ZO-1. With respect to ultrastructural correlates, almost all of those ZO-1/Cx45 double-labeled gap junctions were of the plaque type, and none were strings or ribbons. In contrast, ca. 50% of Cx36-containing gap junctions in the OFF sublamina were string and ribbon configurations, and those were shown to be relatively deficient in ZO-1 (Kamasawa et al., 2006; Ciolofan et al., 2006). For plaque gap junctions, ZO-1 labeling was usually present across the gap junction plaques (Fig. 9A,B), whereas connexin labeling was often concentrated near the periphery (Fig. 3A-C, 9A,B), possibly reflecting reduced penetration of anti-connexin antibodies into the gap junctional “cytoplasmic semi-dense matrix” (Sotelo and Korn, 1978; Kosaka and Kosaka, 2003) that is formed by ZO-1 and other scaffolding and accessory proteins (diagrammed in Fig. 9E). Given that IgG molecules are approximately 8x12x12 nm (Valentine and Green, 1967; Huber et al., 1976), or larger than the attached 6-nm or 10-nm gold beads, these cytoplasmic matrix proteins may also reduce immunofluorescence IgG labeling in strongly-fixed sections.

Interaction of Cx45 with ZO-1 in HeLa cells and retina

Cultured HeLa cells stably transfected with Cx45 were used to document Cx45 association with ZO-1. In control empty-vector-transfected cells, labeling of ZO-1 typically appeared as fine, intermittent puncta or as short, continuous strands of immunofluorescence at cell-cell contacts (Fig. 10A1), whereas Cx45 immunoreactivity was entirely absent (Fig. 10A2, 10A3). In Cx45-HeLa cells, labeling of ZO-1 had a more dispersed appearance and was localized both at cell-cell contacts as well as intracellularly (Fig. 10B1). Nearly all cells displayed labeling of Cx45 in puncta at contacts between cells and/or intracellularly (Fig. 10B2). Double immunofluorescence labeling indicated partial Cx45/ZO-1 overlap at both of these subcellular locations (Fig. 10B3). Laser scanning confocal double immunofluorescence imaging further revealed that individual ZO-1-positive puncta at cell margins were immunopositive for Cx45 (Fig. 10C).

Immunoblotting and co-immunoprecipitation were used to confirm anti-Cx45 antibody specificity and to examine molecular interaction of Cx45 with ZO-1. In lysates of Cx45-HeLa cells examined using 12.5% gels, monoclonal anti-Cx45 (Millipore/Chemicon) detected a band migrating at approximately 45 kDa (Fig. 11A, lane 2), whereas this band was absent in empty vector-transfected HeLa cells (Fig. 11A, lane 1). A similar co-migrating band was detected in homogenates of retina (Fig. 11A, lane 4), but was absent in homogenates of liver (Fig. 11A, lane 3), which was used as a negative control. After IP of ZO-1 from homogenates of retina using polyclonal anti-ZO-1, IP material probed with monoclonal anti-Cx45 was found to contain Cx45 (Fig. 11A, lane 6) co-migrating with corresponding bands detected with monoclonal anti-Cx45 in retina (5% of input protein in IP) and in Cx45-HeLa cells. Cx45 was not detectable in immunoblotted material after omission of anti-ZO-1 in the IP procedure (Fig. 11A, lane 5). A separate blot again shows a Cx45 band in retina (Fig. 11A, lane 7) and absence of this band after IP of ZO-1 from retina using anti-FLAG IgG as control antibody (Fig. 11A,

lane 8). By western blotting, we have previously shown the presence of ZO-1 in retinal homogenates used as input for IP of ZO-1 (Li et al., 2004a). Immunoblotting of Cx45-HeLa cells using 12.5% gels and probing of membranes with polyclonal anti-Cx45 gave a similar detection of Cx45 (Fig. 11B, lane 1), which was absent in empty vector-transfected cells (Fig. 11B, lane 2). In 10% SDS-gels, the polyclonal anti-Cx45 detected a doublet of bands (Fig. 11C), corresponding in molecular weight to previously reported phosphorylated and non-phosphorylated forms of Cx45 (van Veen et al., 2000). The polyclonal anti-Cx45 also detected Cx45 obtained from retina after IP of Cx45 with monoclonal anti-Cx45 (Fig. 11D). These data demonstrated similar labeling specificity for all Cx45 antibodies tested.

Homogenates of mouse retina were used with fusion proteins containing GST linked separately to each of the three PDZ domains in ZO-1 for in vitro pull-down assays to examine direct binding of Cx45 to the PDZ domains of ZO-1. As shown by immunoblotting (Fig. 12A), eluates of protein from beads coupled to either the GST-PDZ1 (Fig. 12A, lane 2) or GST-PDZ3 (Fig. 12A, lane 4) domain of ZO-1 were devoid of Cx45, whereas protein eluted from beads coupled to the GST-PDZ2 domain of ZO-1 (Fig. 12A, lane 3) contained Cx45, which migrated as a band corresponding to Cx45 detected in homogenates of mouse retina (Fig. 12A, lane 1). Stripping of the blot in Fig. 12A and re-probing with anti-GST antibody revealed equal loading of the three PDZ domain fusion proteins (Fig. 12B). As a positive control for the functional binding capacity of the PDZ1 domain fusion protein, we have previously shown that this fusion protein was able to bind to the c-terminus of Cx36 in pull-down assays (Li et al., 2004a,b).

Co-IP of Cx36 with Cx45 from retina and HeLa cells

Direct interaction of Cx36 with the PDZ1 domain of ZO-1 and interaction of Cx45 with the PDZ2 domain of ZO-1, together with the presence of these two connexins in the same gap junctional hemiplaques, raised the possibility that these two connexins may be linked together by ZO-1 in a tripartite complex. Molecular association of Cx36 with Cx45 was therefore investigated by co-IP of these connexins from mouse retina and from HeLa cells co-transfected with either full-length Cx36 and Cx45 or with full-length Cx45 and truncated Cx36 (Cx36tr) lacking the c-terminus PDZ1 domain binding motif. As shown in immunoblots probed with polyclonal anti-Cx36, IP of Cx45 with monoclonal anti-Cx45 resulted in detection of Cx36 in retinal IP material (Fig. 13A, lane 2) and in IP material from HeLa cells co-transfected with Cx36/Cx45 (Fig. 13A, lane 1). In contrast, Cx36 was not detected in IP material from HeLa cells co-transfected with Cx45 and truncated Cx36 (Fig. 13A, lane 3), nor was it detected in IP material after omission of anti-Cx45 during the IP procedure (Fig. 12A, lane 4). We have previously shown by western blotting that truncation of Cx36 by four c-terminus amino acids still allows Cx36 recognition by polyclonal anti-Cx36 antibody (Li et al., 2004a). Similar results were obtained using the reverse IP approach; IP of Cx36 with polyclonal anti-Cx36 resulted in detection of Cx45 in retinal IP material when probed with monoclonal anti-Cx45 (Fig. 13B, lane 2) and detection of Cx45 in IP material from Cx36/Cx45 co-transfected HeLa cells (Fig. 13B, lane 1). However, Cx45 was not detected in IP material from HeLa cells co-transfected with Cx45 and truncated Cx36 (Fig. 13B, lane 3) or in IP material after omission of anti-Cx36 during the IP procedure (Fig. 12B, lane 4). Additional control procedures are shown in supplementary Fig. S2. Specifically, input levels of Cx36 and Cx45 are demonstrated in lysates (5%) of Cx36/Cx45-transfected and Cx36-tr/Cx45-transfected HeLa cells and retinal homogenates used for co-IP, and absence of Cx45 or Cx36 in IP material is shown after IP from each of the tissues using monoclonal and polyclonal anti-FLAG antibodies as control IgG.

Discussion

Establishing neuronal gap junctional coupling relationships in the retina is essential for understanding how rod scotopic and mesopic information is “piggybacked” onto the photopic cone pathway (Kolb, 1979; Strettoi et al., 1992; Vaney, 2002). Key to this goal is identification of connexin expression profiles of IPL neurons and determination of the connexin constituents of their gap junctions. A major new finding from FRIL and from SDS-FRL double-replicas, and one entirely unexpected based on current literature descriptions of neuron subtype-specific expression of Cx36 vs. Cx45 in the IPL of rodent retina, is that Cx36 was nearly always co-localized with Cx45 in Cx45-containing freeze-fractured neuronal gap junctions. If a significant fraction of retinal gap junctions in IPL were to express only Cx45 in homotypic or in heterotypic hemiplaques, as proposed by others, FRIL would have revealed primarily or exclusively Cx45-single-labeled hemiplaques. This was not observed. Suggestions that Cx45 does not form functional heterotypic couplings with Cx36 (Teubner et al., 2000) were further supported by our co-expression experiments, which showed absence of heterotypic puncta in HeLa cells expressing Cx45 and Cx36. Overall, our finding that 87% of Cx45-immunopositive puncta in the IPL were also immunopositive for Cx36 supports the extent of Cx36/Cx45 co-localization across the IPL. Finally, Cx45- and Cx36 often had segregated but mirror distributions in both sides of opposing hemiplaques, forming definitive bi-homotypic rather than heterotypic gap junctions, and moreover, that Cx45 and Cx36 were primarily or exclusively in homomeric connexons. These results raise several issues regarding current literature on connexin biology in the IPL.

First, Cx45-positive immunofluorescent puncta in the IPL were reported never to overlap (0%) with Cx36-positive puncta (Han and Massey, 2005) or to exhibit 30% co-localization (Dedek et al., 2006), both contrasting with 87% immunofluorescence co-localization found here. Likewise, the OFF sublamina was reported to be devoid of Cx45-immunofluorescence (Güldenagel et al., 2000) or to contain a very low density of Cx45 (Maxeiner et al., 2005) – where we observed relatively abundant Cx45 puncta. Also contradictory, Feigenspan et al. (2001) noted that the heterologous gap junctions between AII amacrine cells and ON cone bipolar cells “appear to be heterotypic because ON cone bipolar cells do not express Cx36”, whereas Deans et al. (2002) stated that “Cx36 is expressed by ON CBs coupled to AII amacrine cells”. In contrast, Maxeiner et al. (2005) stated that “all four classes of OFF cone bipolar cells express Cx45”, and acknowledged “the possibility that both Cx36 and Cx45 are expressed by the same bipolar cell.” We attribute these differences in immunofluorescence detection to fixation-dependent reduction in antibody labeling, as evidenced by a lower percentage of Cx36/Cx45 co-localization after increased fixation (45% vs. 87%).

Second, reporter-based approaches to cell-type identification of connexin expression in IPL suggested that neurons expressing Cx45 represent entirely different populations than those expressing Cx36. Thus, Dedek et al. (2006) attributed their 30% co-localization of Cx36 with Cx45 to each connexin exclusively in opposite sides of opposed hemiplaques, which they proposed to represent heterotypic Cx45-cone bipolar to Cx36-AII amacrine cell gap junctions. Although Cx45 lacks dye-coupling competence with Cx36 in HeLa cells transfected with these connexins (Teubner et al., 2000), it was suggested that HeLa cells might lack essential accessory proteins that otherwise permit the hypothesized functional Cx36/Cx45 coupling in IPL neurons (Maxeiner et al., 2005). Because Teubner and coworkers had not assayed for connexin co-localization, we investigated similar connexin-transfected HeLa cell lines and showed that they form immunopositive plaques containing homotypic Cx36/Cx36, Cx43/Cx43, and Cx45/Cx45 puncta, as well as heterotypic Cx43/Cx45 puncta at cell-cell abutments, but did not form heterotypic Cx45/Cx36 puncta. Instead, immunofluorescence co-localization of Cx45+Cx36 in HeLa cell contacts required that both cells simultaneously co-express both proteins. Because HeLa cells contain requisite scaffolding and targeting proteins to allow

separate formation of Cx45-containing and Cx36-containing gap junctions, as well as Cx45 +Cx36 bi-homotypic gap junctions, Cx45 appears unable to form heterotypic puncta with Cx36 in these cells.

Third, our combined results imply that Cx45 and Cx36 are transported to and stabilized in retinal gap junctions by common targeting and scaffolding proteins. Cx36 binds to the PDZ1 domain of ZO-1 (Li et al., 2004a,b), and here we showed Cx45/ZO-1 co-association in mouse retina and interaction of Cx45 with the PDZ2 domain, which had not been determined previously (Kausalya et al, 2001; Laing et al., 2001; Thomas et al., 2002). Significantly, Cx45/ZO-1 co-localization persisted in IPL from Cx36 ko mice, indicating that this co-localization was not simply due to ZO-1 association with Cx36 at Cx36/Cx45-containing gap junctions. Presence of all three proteins in IPL gap junctions and their co-IP suggest an essential targeting and scaffolding role for ZO-1 in Cx45+Cx36-containing gap junctions. With nine members of the connexin family of proteins reported to associate with ZO-1 (Giepmans, 2004; Li et al., 2004a,b,c; Penes et al., 2005), a regulatory role for ZO-1 at gap junctions is emerging (Li et al., 2004a,b,c; Laing et al., 2005; Hunter et al., 2005; Akoyev and Takemoto, 2007). Binding of Cx36 and Cx45 to different ZO-1 PDZ domains suggests that ZO-1 may simultaneously interact with Cx36 and Cx45 in a tripartite fashion, thereby tethering the two connexins within gap junctions. A critical role of ZO-1 in mediating this association was indicated by abolition of Cx36/Cx45 co-IP after removal of the c-terminus four amino acid residues of Cx36 (this report), which are required for the interaction of Cx36 with the PDZ1 domain of ZO-1 (Li et al., 2004a).

Fourth, heterotypic gap junctional coupling between Cx36-expressing AII amacrine cells and Cx45-expressing ON-cone bipolar cells was advanced as a key element in the rod pathway, based on substantial alteration of electroretinograms in Cx45 ko mice (Maxeiner et al., 2005). We found that absence of Cx36 in Cx36 ko mice was accompanied by 25% reduction of Cx45-puncta in IPL. Our results, combined with those of Maxeiner et al. (2005), suggest that reduced coupling observed in this pathway after Cx36 ko (Güldenagel et al., 2001; Deans et al., 2002) may be due to loss of not only Cx36, but also to a small reduction in Cx45 expression or trafficking, which may require Cx45 co-binding with Cx36 and ZO-1 for optimum targeting and/or stability. Because Cx45-containing gap junctions appear to obligately contain Cx36, knockout of Cx45 from these otherwise bi-homotypic gap junctions also might alter the function and/or stability of the Cx36 that remains in the absence of Cx45.

Fifth, previous studies suggested that most if not all neurons synapsing in the IPL separately express only one or the other connexin isoform (Han and Massey, 2005; Dedek et al., 2006). However, the methods used, including *in situ* hybridization, single-cell RT-PCR, lacZ reporter expression (by a non-conventional method; Schubert, et al., 2005), or expression of cytoplasmic EGFP as genetic markers (Maxeiner et al., 2005; Lin et al., 2005; Han and Massey, 2005; Dedek et al., 2006), have significant probabilities of both “false positive” and “false negative” detection; and as in all techniques, efforts to minimize false positives increase the probability of false negatives by altering the threshold of signal detection. For example, by reducing amplification of lacZ signal so that Cx45-positive cells had from one to a maximum of three lacZ cytoplasmic “dots” (Schubert et al., 2005), weakly-expressing cells may have had inadequate amplification to produce a detectable dot, leading to false negatives. Likewise, none of the mRNA-detection methods measure different expression levels that are implied by vastly different sizes (and numbers) of Cx36- vs. Cx45/Cx36-containing gap junctions (4-2500 connexons; Kamasawa et al, 2006). Our data imply that AII amacrine cells, reportedly expressing only Cx36 (Maxeiner et al., 2005), that couple to Cx45/Cx36 co-expressing cells (e.g., cone bi-polar cells) must form only Cx36/Cx36 mono-homotypic couplings, or that AII amacrine cells must also synthesize Cx45 to form bi-homotypic gap junctions, but with Cx45 synthesized at an amount sufficiently low as to have previously gone undetected. Conversely,

if AII amacrine cells truly lack Cx45, the detection of Cx45-immunofluorescent puncta at apparent cell contacts involving AII amacrine cells must be at tripartite contacts between two other Cx45/Cx36-coexpressing cell processes that are not separately resolvable by light microscopy from the closely-associated AII amacrine cell. Such triadic structural arrangements (Fig. 29b, Kolb, 1979) could also account for the reduction in glycine transfer from AII amacrine cells to cone bipolar cells in both Cx36 and Cx45 ko mice (Güldenagel, et al. 2001; Maxeiner et al. 2005) if the intermediary neuron expressing Cx36+Cx45 were coupled to glycinergic AII amacrine cells solely by Cx36-containing gap junctions and serially to the non-glycinergic bipolar cells by bi-homotypic Cx45/Cx36 gap junctions. Additionally, this would require that Cx45 ko also disrupt Cx45/Cx36 bi-homotypic couplings.

Overall, our results document that virtually all Cx45-containing gap junctions occur between cell pairs in which both cells co-express and co-target Cx45 and Cx36, forming bi-homotypic gap junctions. Thus, interpretation of future coupling experiments involving Cx45-expressing retinal neurons must consider the restricted range of sizes of Cx45-containing gap junctions as compared with homotypic Cx36 gap junctions, rather than ascribing observed differences in coupling to heterotypic vs. homotypic coupling. For example, gating of Cx45 (but not Cx36) is voltage-sensitive, and Cx45 has 3-fold greater conductance (Söhl et al., 2005), potentially allowing differential regulation of gap junction electrical and/or metabolic coupling. Consequently, subcellular regulation of the ratios and abundance of these two connexins in individual gap junctions would allow for finer analog control than available from mono-homotypic Cx36 or Cx45 gap junctions, as well as provide a novel mechanism for plasticity of electrical synapses.

Supplementary Material

Refer to Web version on PubMed Central for supplementary material.

Acknowledgements

This work was supported by grants from the Canadian Institutes of Health Research to JIN, by NIH grants NS31027, NS44010 and NS44395 to JER, and by SORST, Japan Science and Technology Agency to RS. We thank B. McLean for excellent technical assistance, Dr. D. Paul (Harvard University) for providing a breeding pair of Cx36^{+/-} mice, Dr. B. Giepmans (University of California San Diego, CA, USA) for providing GST-PDZ expression vectors, and Dr. K. Willecke (University of Bonn, Bonn, Germany) for providing HeLa cells stably transfected with Cx43 and Cx45. We thank Dr. J. zumBrunnen, Department of Statistics, Colorado State University, for assistance in determination of confidence intervals.

References

- Akoyev V, Takemoto DJ. ZO-1 is required for protein kinase C gamma-driven disassembly of connexin43. *Cell Signal* 2007;19:958–967. [PubMed: 17210245]
- Balda MS, Garrett MD, Matter K. The ZO-1-associated Y-box factor ZONAB regulates epithelial cell proliferation and cell density. *J Cell Biol* 2003;160:423–432. [PubMed: 12566432]
- Challcroft JP, Bullivant S. An interpretation of liver cell membrane and junction structure based on observation of freeze-fracture replicas of both sides of the fracture. *J Cell Biol* 1970;47:49–60. [PubMed: 4935338]
- Chen VC, Li XB, Perreault H, Nagy JI. Interaction of zonula occludens-1 (ZO-1) with alpha-actinin-4: application of functional proteomics for identification of PDZ domain-associated proteins. *J Proteome Res* 2006;5:2123–2134. [PubMed: 16944923]
- Ciolofan C, Li XB, Olson C, Kamasawa N, Gebhardt BR, Yasumura T, Morita M, Rash JE, Nagy JI. Association of connexin36 and zonula occludens-1 with zonula occludens-2 and the transcription factor zonula occludens-1-associated nucleic acid-binding protein at neuronal gap junctions in rodent retina. *Neuroscience* 2006;140:433–451. [PubMed: 16650609]

- Deans MR, Völgyi B, Goodenough DA, Bloomfield SA, Paul DL. Connexin36 is essential for transmission of rod-mediated visual signals in the mammalian retina. *Neuron* 2002;36:703–712. [PubMed: 12441058]
- Dedek K, Schultz K, Pieper M, Dirks P, Maxeiner S, Willecke K, Weiler R, Janssen-Bienhold U. Localization of heterotypic gap junctions composed of connexin45 and connexin36 in the rod pathway of the mouse retina. *Eur J Neurosci* 2006;24:1675–1686. [PubMed: 17004931]
- Dinchuk JE, Johnson TJA, Rash JE. Postreplication labeling of E-leaflet molecules: Membrane immunoglobulins localized in sectioned labeled replicas examined by TEM and HVEM. *J Electron Microscop Tech* 1987;7:1–16. [PubMed: 2464678]
- Elfang C, Eckert R, Lichtenberg-Frate H, Butterweck A, Traub O, Klein RA, Hulser DF, Willecke K. Specific permeability and selective formation of gap junction channels in connexin-transfected HeLa cells. *J Cell Biol* 1995;129:805–817. [PubMed: 7537274]
- Evans WH, Martin PEM. Gap junctions: structure and function. *Mol Membr Biol* 2002;19:121–136. [PubMed: 12126230]
- Feigenspan A, Teubner B, Willecke K, Weiler R. Expression of neuronal connexin36 in AII amacrine cells of the mammalian retina. *J Neurosci* 2001;21:230–239. [PubMed: 11150340]
- Fujimoto K. Freeze-fracture replica electron microscopy combined with SDS digestion for cytochemical labeling of integral membrane proteins. Application to the immunogold labeling of intercellular junctional complexes. *J Cell Sci* 1995;108:3443–3449. [PubMed: 8586656]
- Fujimoto K. SDS-digested freeze-fracture replica labeling electron microscopy to study the two-dimensional distribution of integral membrane proteins and phospholipids in biomembranes: practical procedure, interpretation and application. *Histochem Cell Biol* 1997;107:87–96. [PubMed: 9062793]
- Fujimoto K, Nagafuchi A, Tsukita Sh, Kuraoka A, Ohokuma A, Shibata Y. Dynamics of connexins, E-cadherin, and α -catenin on cell membranes during gap junction formation. *J Cell Sci* 1997;110:311–322. [PubMed: 9057084]
- Gaietta G, Deerinck TJ, Adams SR, Bouwer J, Tour O, Laird DW, Sosinsky GE, Tsien RY, Ellisman MH. Multicolor and electron microscopic imaging of connexin trafficking. *Science* 2002;296:503–507. [PubMed: 11964472]
- Ghosh KK, Buojan S, Haverkamp S, Feigenspan A, Wassle H. Types of bipolar cells in the mouse retina. *J Comp Neurol* 2004;469:70–82. [PubMed: 14689473]
- Giepman BN. Gap junctions and connexin-interacting proteins. *Cardiovasc Res* 2004;62:233–245. [PubMed: 15094344]
- Grujters WTM, Kistler J, Bullivant S, Goodenough DA. Immunolocalization of MP70 in lens fiber 16-17-nm intercellular junctions. *J Cell Biol* 1987;104:565–572. [PubMed: 3818793]
- Güldenagel M, Söhl G, Plum A, Traub O, Teubner B, Weiler R, Willecke K. Expression patterns of connexin genes in mouse retina. *J Comp Neurol* 2000;425:193–201. [PubMed: 10954839]
- Güldenagel M, Ammermüller J, Feigenspan A, Teubner B, Degen J, Söhl G, Willecke K, Weiler R. Visual transmission deficits in mice with targeted disruption of the gap junction gene connexin36. *J Neurosci* 2001;21:6036–6044. [PubMed: 11487627]
- Han Y, Massey SC. Electrical synapses in retinal ON cone bipolar cells: subtype-specific expression of connexins. *Proc Natl Acad Sci USA* 2005;102:13313–13318. [PubMed: 16150718]
- Huber R, Deisenhofer J, Colman PM, Matsushima M, Palm W. Crystallographic structure studies of an IgG molecule and an Fc fragment. *Nature* 1976;264:415–420. [PubMed: 1004567]
- Hunter AW, Barker RJ, Zhu C, Gourdie RG. Zonula occludens-1 alters connexin43 gap junction size and organization by influencing channel accretion. *Mol Biol Cell* 2005;16:5686–5698. [PubMed: 16195341]
- Kamasawa N, Furman CS, Davidson KGV, Sampson JA, Magnie AR, Gebhardt BR, Kamasawa M, Yasumura T, Zumbrennen JR, Pickard GE, Nagy JI, Rash JE. Abundance and ultrastructural diversity of neuronal gap junctions in the OFF and ON sublaminae of the inner plexiform layer of rat and mouse retina. *Neuroscience* 2006;142:1093–1117. [PubMed: 17010526]
- Kamasawa N, Sik A, Morita M, Yasumura T, Davidson KGV, Nagy JI, Rash JE. Connexin47 and connexin32 in gap junctions of oligodendrocyte somata, myelin sheaths, paranodal loops, and

- Schmidt-Lanterman incisures: Implications for ionic homeostasis and potassium siphoning. *Neuroscience* 2005;136:65–86. [PubMed: 16203097]
- Kausalya PJ, Reichert M, Hunziker W. Connexin45 directly binds to ZO-1 and localizes to the tight junction region in epithelial MDCK cells. *FEBS Lett* 2001;505:92–96. [PubMed: 11557048]
- Kolb H. The inner plexiform layer in the retina of the cat: electron microscopic observations. *J Neurocytol* 1979;8:295–329. [PubMed: 490185]
- Kolb H, Famiglietti EV. Rod and cone pathways in the inner plexiform layer of cat retina. *Science* 1974;186:47–49. [PubMed: 4417736]
- Kosaka T, Kosaka K. Neuronal gap junctions in the rat main olfactory bulb, with special reference to intraglomerular gap junctions. *Neurosci Res* 2003;45:189–209. [PubMed: 12573466]
- Kruger O, Plum A, Kim JS, Winterhager E, Maxeiner S, Hallas G, Kirchhoff S, Traub O, Lamers WH, Willecke K. Defective vascular development in connexin45-deficient mice. *Development* 2000;127:4179–4193. [PubMed: 10976050]
- Laing JG, Manley-Markowski RN, Koval M, Civitelli R, Steinberg TH. Connexin45 interacts with zonula occludens-1 and connexin43 in osteoblastic cells. *J Biol Chem* 2001;276:23051–23055. [PubMed: 11313345]
- Laing JG, Chou BC, Steinberg TH. ZO-1 alters the plasma membrane localization and function of Cx43 in osteoblastic cells. *J Cell Sci* 2005;118:2167–2176. [PubMed: 15855237]
- Li X, Simard JM. Connexin45 gap junction channels in rat cerebral vascular smooth muscle cells. *Am J Physiol* 2001;281:H1890–H1898.
- Li X, Olson C, Lu S, Kamasawa N, Yasumura T, Rash JE, Nagy JI. Neuronal connexin36 association with zonula occludens-1 protein (ZO-1) in mouse brain and interaction with the first PDZ domain of ZO-1. *Eur J Neurosci* 2004a;19:2132–2146. [PubMed: 15090040]
- Li X, Olson C, Lu S, Nagy JI. Association of connexin36 with zonula occludens-1 in HeLa cells, β TC-3 cells, pancreas and adrenal gland. *Histochem Cell Biol* 2004b;122:485–498. [PubMed: 15558297]
- Li X, Ionescu AV, Lynn BD, Lu S, Kamasawa N, Morita M, Davidson KG, Yasumura T, Rash JE, Nagy JI. Connexin47, connexin29 and connexin32 co-expression in oligodendrocytes and Cx47 association with zonula occludens-1 (ZO-1) in mouse brain. *Neuroscience* 2004c;126:611–630. [PubMed: 15183511]
- Lin B, Jakobs TC, Masland RH. Different functional types of bipolar cells use different gap-junctional proteins. *J Neurosci* 2005;25:6696–6701. [PubMed: 16014731]
- Masugi-Tokita M, Tarusawa E, Watanabe M, Molnar E, Fujimoto K, Shigemoto R. Number and density of AMPA receptors in individual synapses in the rat cerebellum as revealed by SDS-digested freeze-fracture replica labeling. *J Neurosci* 2007;27:2135–2144. [PubMed: 17314308]
- Maxeiner S, Dedek K, Janssen-Bienhold J, Ammermuller J, Brune H, Kirsch T, Pieper M, Degen J, Kruger O, Willecke K, Weiler R. Deletion of connexin45 in mouse retinal neurons disrupts the rod/cone signaling pathway between AII amacrine and ON cone bipolar cells and leads to impaired visual transmission. *J Neurosci* 2005;19:566–576. [PubMed: 15659592]
- Meier C, Dermietzel R, Davidson KGV, Yasumura T, Rash JE. Connexin32-containing gap junctions in Schwann cells at the internodal zone of partial myelin compaction and in Schmidt-Lanterman incisures. *J Neurosci* 2004;24:3186–3198. [PubMed: 15056698]
- Nagy JI, Dudek FE, Rash JE. Update on connexins and gap junctions in neurons and glia in the nervous system. *Brain Res Rev* 2004;47:191–215. [PubMed: 15572172]
- Nielsen PA, Beahm DL, Giepmans BN, Baruch A, Hall JE, Kumar NM. Molecular cloning, functional expression, and tissue distribution of a novel human gap junction-forming protein, connexin31.9. Interaction with zona occludens protein-1. *J Biol Chem* 2002;277:38272–38283. [PubMed: 12154091]
- Nielsen PA, Baruch A, Shestopalov VI, Giepmans BN, Benedetti EI, Kumar NM. Lens connexins Cx46 and Cx50 interact with Zonula Occludens Protein-1 (ZO-1). *Mol Biol Cell* 2003;14:2470–2481. [PubMed: 12808044]
- Penes M, Li X, Nagy JI. Expression of zonula occludens-1 (ZO-1) and the transcription factor ZO-1-associated nucleic acid-binding protein (ZONAB/MsY3) in glial cells and co-localization at oligodendrocyte and astrocyte gap junctions in mouse brain. *Eur J Neurosci* 2005;22:404–418. [PubMed: 16045494]

- Rackauskas M, Kreuzberg MM, Pranevicius M, Willecke K, Verselis VK, Bukauskas FF. Gating properties of heterotypic gap junction channels formed of connexins 40, 43 and 45. *Biophys J* 2007;92:1952–1965. [PubMed: 17189315]
- Rash JE, Dillman RK, Bilhartz BL, Duffy HS, Whalen LR, Yasumura T. Mixed synapses discovered and mapped throughout mammalian spinal cord. *Proc Natl Acad Sci (USA)* 1996;93:4235–4239. [PubMed: 8633047]
- Rash, JE.; Dillman, RK.; Morita, M.; Whalen, LR.; Guthrie, PB.; Fay-Guthrie, D.; Wheeler, DW. Grid-mapped freeze fracture: Correlative confocal laser scanning microscopy and freeze-fracture electron microscopy of preselected cells in tissue slices. In: Severs, NJ.; Shotton, DM., editors. *Rapid Freezing, Freeze Fracture, and Deep Etching*. New York, NY: Wiley-Liss, Inc.; 1995. p. 127-150.
- Rash JE, Duffy HS, Dudek FE, Bilhartz BL, Whalen LR, Yasumura T. Grid-mapped freeze-fracture analysis of gap junctions in gray and white matter of adult rat central nervous system, with evidence for a “panglial syncytium” that is not coupled to neurons. *J Comp Neurol* 1997;388:265–292. [PubMed: 9368841]
- Rash JE, Olson C, Davidson KGV, Yasumura T, Kamasawa N, Nagy JI. Identification of connexin36 in gap junctions between neurons in rodent locus coeruleus. *Neuroscience* 2007a;147:938–956. [PubMed: 17601673]
- Rash JE, Olson CO, Pouliot WA, Davidson KGV, Yasumura T, Furman CS, Royer S, Kamasawa N, Nagy JI, Dudek FE. Connexin36, miniature neuronal gap junctions, and limited electrotonic coupling in rodent suprachiasmatic nucleus. *Neuroscience* 2007b;149:350–371. [PubMed: 17904757]
- Rash JE, Pereda A, Kamasawa N, Furman CS, Yasumura T, Davidson KGV, Dudek FE, Olson C, Li X, Nagy JI. High-resolution proteomic mapping in the vertebrate central nervous system: Close proximity of connexin35 to NMDA glutamate receptor clusters and co-localization of connexin36 with immunoreactivity for zonula occludens protein-1 (ZO-1). *J Neurocytol* 2004;33:131–151. [PubMed: 15173637]
- Rash JE, Yasumura T. Direct immunogold labeling of connexins and aquaporin4 in freeze-fracture replicas of liver, brain and spinal cord: factors limiting quantitative analysis. *Cell Tissue Res* 1999;296:307–321. [PubMed: 10382274]
- Rash JE, Yasumura T, Dudek FE, Nagy JI. Cell-specific expression of connexins and evidence of restricted gap junctional coupling between glial cells and between neurons. *J Neurosci* 2001;15:1983–2000. [PubMed: 11245683]
- Schubert T, Maxeiner S, Kruger O, Willecke K, Weiler R. Connexin45 mediates gap junctional coupling of bistratified ganglion cells in the mouse retina. *J Comp Neurol* 2005;490:29–39. [PubMed: 16041717]
- Söhl G, Maxeiner S, Willecke K. Expression and functions of neuronal gap junctions. *Nat Rev Neurosci* 2005;6:191–200. [PubMed: 15738956]
- Söhl G, Willecke K. An update on connexin genes and their nomenclature in mouse and man. *Cell Adhes Comm* 2003;10:173–180.
- Sotelo C, Korn H. Morphological correlates of electrical and other interactions through low-resistance pathways between neurons of the vertebrate central nervous system. *Internat Rev Cytol* 1978;55:67–107.
- Steere RL, Erbe EF. Supporting freeze-etch specimens with ‘Lexan’ while dissolving biological remains in acids. *Microscopy Society of America Proceedings* 1983;41:618–619.
- Strettoi E, Raviola E, Dacheux RF. Synaptic connections of the narrow-field, bistratified rod amacrine cell (AII) in the rabbit retina. *J Comp Neurol* 1992;325:152–168. [PubMed: 1460111]
- Tanaka, Ji; Matsuzaki, M.; Tarusawa, E.; Momiyama, A.; Molnar, E.; Kasai, H.; Shigemoto, R. Number and density of AMPA receptors in single synapses in immature cerebellum. *J Neurosci* 2005;25:799–807. [PubMed: 15673659]
- Teubner B, Degen J, Söhl G, Guldenagel M, Bukauskas FF, Trexler EB, Verselis VK, De Zeeuw CI, Lee CG, Kozak CA, Petrasch-Parwez E, Dermietzel R, Willecke K. Functional expression of the murine connexin 36 gene coding for a neuron-specific gap junctional protein. *J Membr Biol* 2000;176:249–262. [PubMed: 10931976]

- Thomas MA, Huang S, Cokoja A, Riccio O, Staub O, Suter S. Interaction of connexins with protein partners in the control of channel turnover and gating. *Biol Cell* 2002;94:445–456. [PubMed: 12566219]
- Valentine RC, Green NM. Electron microscopy of an antibody-hapten complex. *J Mol Biol* 1967;27:615–617. [PubMed: 4167449]
- van den Pol AN, Ghosh PK, Liu Rj, Li Y, Aghajanian GK, Gao XB. Hypocretin (orexin) enhances neuron activity and cell synchrony in developing mouse GFP-expressing locus coeruleus. *J Physiol* 2002;541:169–185. [PubMed: 12015428]
- Vaney DI. Retinal neurons: cell types and coupled networks. *Prog Brain Res* 2002;136:239–254. [PubMed: 12143385]
- Vaney DI, Weiler R. Gap junctions in the eye: evidence for heteromeric, heterotypic and mixed-homotypic interactions. *Brain Research Reviews* 2000;32:115–120. [PubMed: 10751660]
- van Veen TA, van Rigen HV, Jongasma HJ. Electrical conductance of mouse connexin45 gap junction channels is modulated by phosphorylation. *Cardiovasc Res* 2000;46:496–510. [PubMed: 10912460]

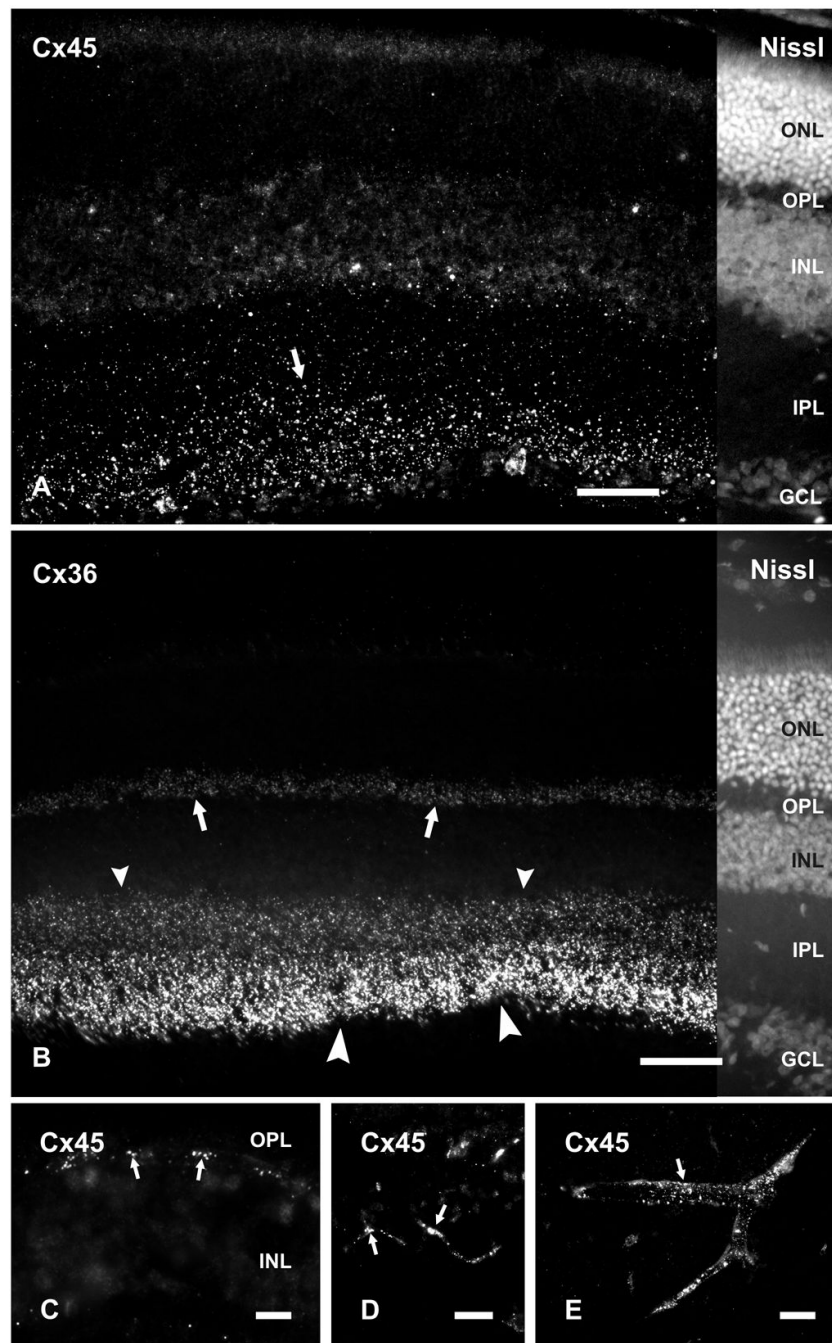


Figure 1.

Immunolabeling of Cx45 and Cx36 in adult mouse retina. **A, B**, Vertical retinal sections labeled by immunofluorescence, with the right portion of each field shown by counterstaining with fluorescent NeuroTrace. Punctate labeling with polyclonal anti-Cx45 is seen in the inner half of the IPL (**A**, arrow), and more sparsely in the outer half of the IPL (**A**). Labeling of Cx36 is very dense in the inner half of the IPL (**B**, large arrowheads), less dense in the outer half of the IPL (**B**, small arrowheads) and moderate in the OPL (**B**, arrows). **C-E**, Higher magnifications showing punctate labeling for Cx45 at the outer margin of the INL (**C**, arrows), and along blood vessels in the retina (**D**, arrows), and in cerebral cortex (**E**, arrow). ONL, outer nuclear layer;

OPL, outer plexiform layer; INL, inner nuclear layer; IPL, inner plexiform layer; GCL, ganglion cell layer. Scale bars, 50 μ m.

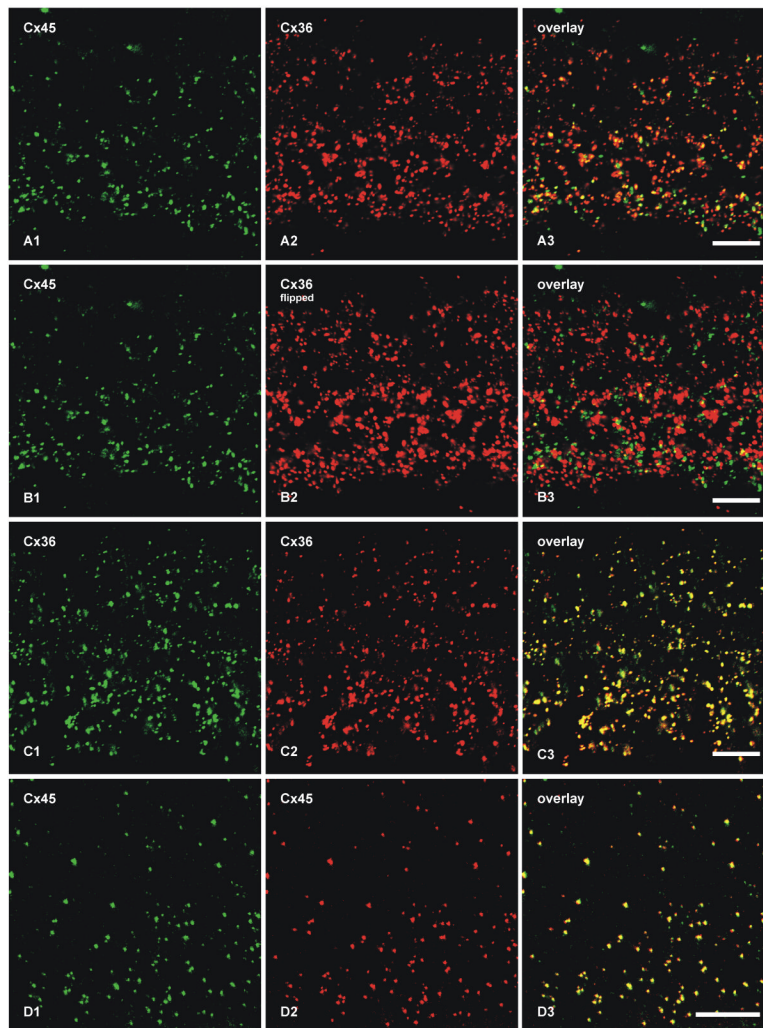


Figure 2. Double-immunofluorescence images showing co-localization of Cx45 with Cx36 in vertical sections of the IPL of adult mouse retina. Images in **A-D** show the entire vertical span of IPL in single confocal scans. **A**, The same field (**A1-A3**) labeled with monoclonal anti-Cx45 and polyclonal anti-Cx36, showing Cx45-positive puncta labeled for Cx36 in retina after perfusion of mice with 20 ml of tissue fixative. **B**, The same set of confocal double immunofluorescence images as in **A**, showing minimal Cx45/Cx36 co-localization in the IPL after horizontal flipping of the image showing labeling for Cx36. **C**, The same field (**C1-C3**) of IPL double-labeled for Cx36 with monoclonal Ab37-4600 and polyclonal Ab36-4600, showing nearly total overlap of immunopositive puncta. **D**, The same field (**D1-D3**) in a tangential section through the IPL double-labeled for Cx45 with monoclonal MAB3101 and polyclonal Ab40-7000, showing nearly total overlap of immunopositive puncta. Scale bars, 10 μ m.

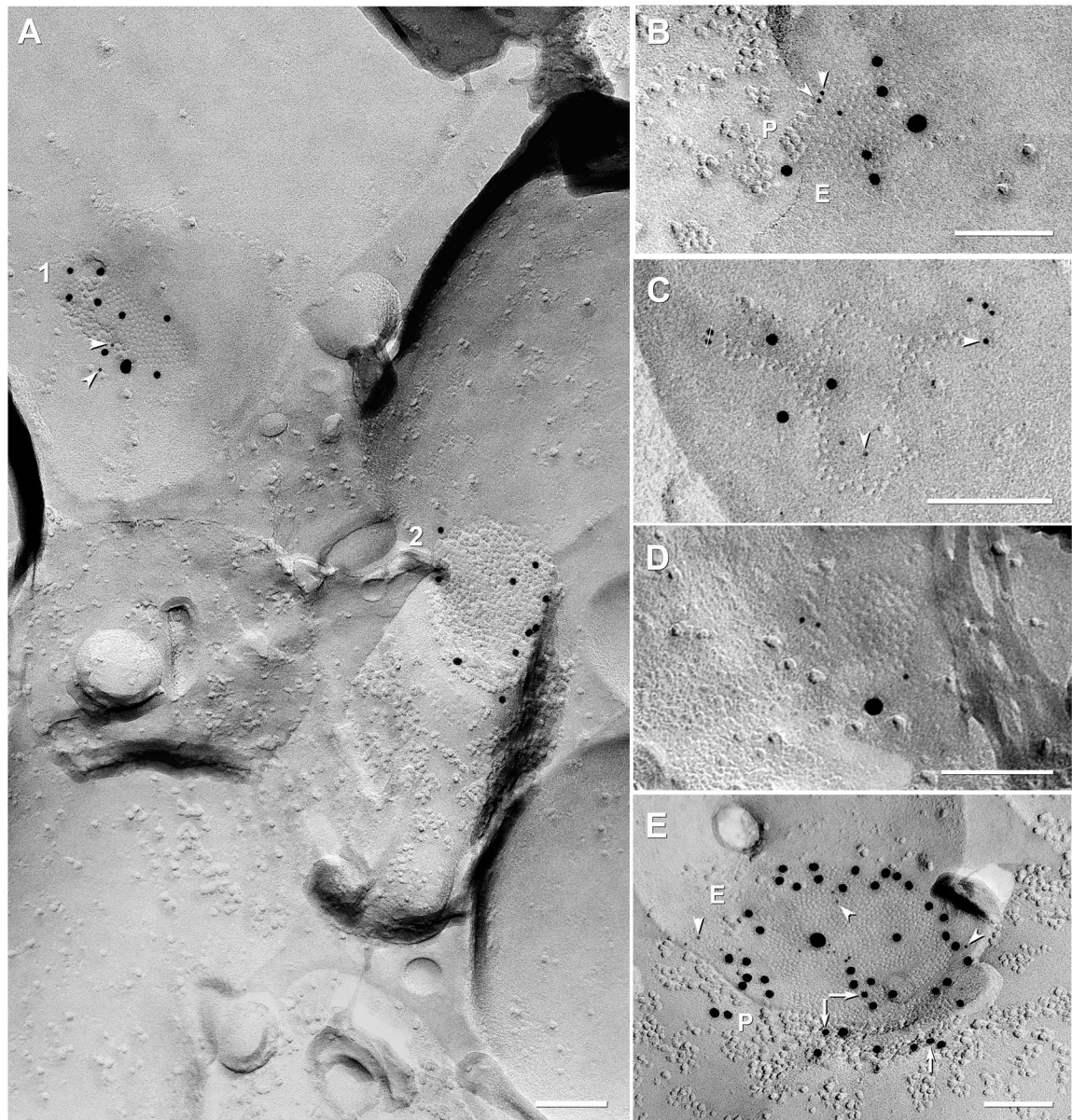


Figure 3.

FRIL localization of Cx45 vs. Cx36 in mouse (A-D) and rat (E) IPL. **A**, Neuronal gap junctions in adjacent cells, one of which (1; 210 connexons) is labeled for both Cx45 (one 18-nm gold and two 6-nm gold beads, arrowheads) and Cx36 (ca. 450 connexons; eight 12-nm gold beads) and the second (2) is labeled for Cx36 only (10 12-nm gold beads). #1 overall LE = 1:19 and #2 LE = 1:45. **B**, Medium-size plaque gap junction (139 connexons) labeled for Cx45 (three 6-nm gold beads, arrowheads, and one 18-nm gold bead) and Cx36 (five 12-nm gold beads); overall LE = 1:15. **C**, Medium-size reticular gap junction (106 connexons) labeled for Cx45 (six 6-nm, arrowheads) and for Cx36 (three 12-nm gold beads). Two gold beads (thin cross-bars) within the apparent “radius of uncertainty” for connexon labeling represent “false-positive” labeling (*i.e.*, “noise”) because stereoscopic analysis (not shown) revealed that both were $>1 \mu\text{m}$ above the replica on an unstable wisp of undissolved Lexan plastic. Overall LE = 1:12. **D**, Small gap junction (68 connexons) in rat IPL labeled for Cx45 only (one 18-nm and three 6-nm gold beads; zero 12-nm gold beads are present for Cx36). Cx45 LE = 1:17. This

gap junction may be too small to allow positive analysis regarding Cx36. *A* and *C* from same replica. *E*, Large plaque gap junction (797 connexons) with small area of P-face and larger area of E-face; labeled for both Cx45 (three 12-nm gold beads, arrows; and one 30-nm gold bead) and for Cx36 (17 6-nm gold beads; arrowheads and 41 18-nm gold beads; labeled for ca. twice as long as all other FRIL images shown; see MATERIALS AND METHODS for details). Overall LE = 1:13. Scale bars, 0.1 μm .

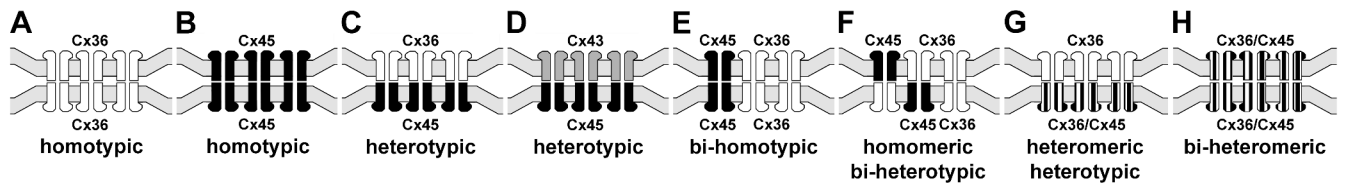


Fig. 4.

Eight generalized connexin/connexon configurations proposed to occur within neuronal gap junctions. **A**, **B**, Homomeric homotypic Cx36-to-Cx36 channels (**A**) and Cx45-to-Cx45 channels (**B**). **C**, Cx36 in the upper cell and Cx45 in the lower cell, with Cx36 linking to Cx45 (“homomeric heterotypic”). **D**, Cx43 in the upper cell and Cx45 in the lower cell, with Cx43 linking to Cx45 (“homomeric heterotypic”). **E**, Both Cx36 and Cx45 in both cells, with Cx36 linked only to Cx36 and Cx45 linked only to Cx45 (“homomeric bi-homotypic”). **F**, Both Cx36 and Cx45 in both cells, with both connexins on one side linked to both connexins on the other side (“homomeric bi-heterotypic”). **G**, Cx36 only in the upper cells linking to connexons containing a mixture of Cx36/Cx45 in the lower cell (homomeric to heteromeric channels). **H**, Each connexon contains both Cx36 and Cx45 (heteromeric connexons), linking to heteromeric connexons in the other cell (heteromeric to heteromeric channels).

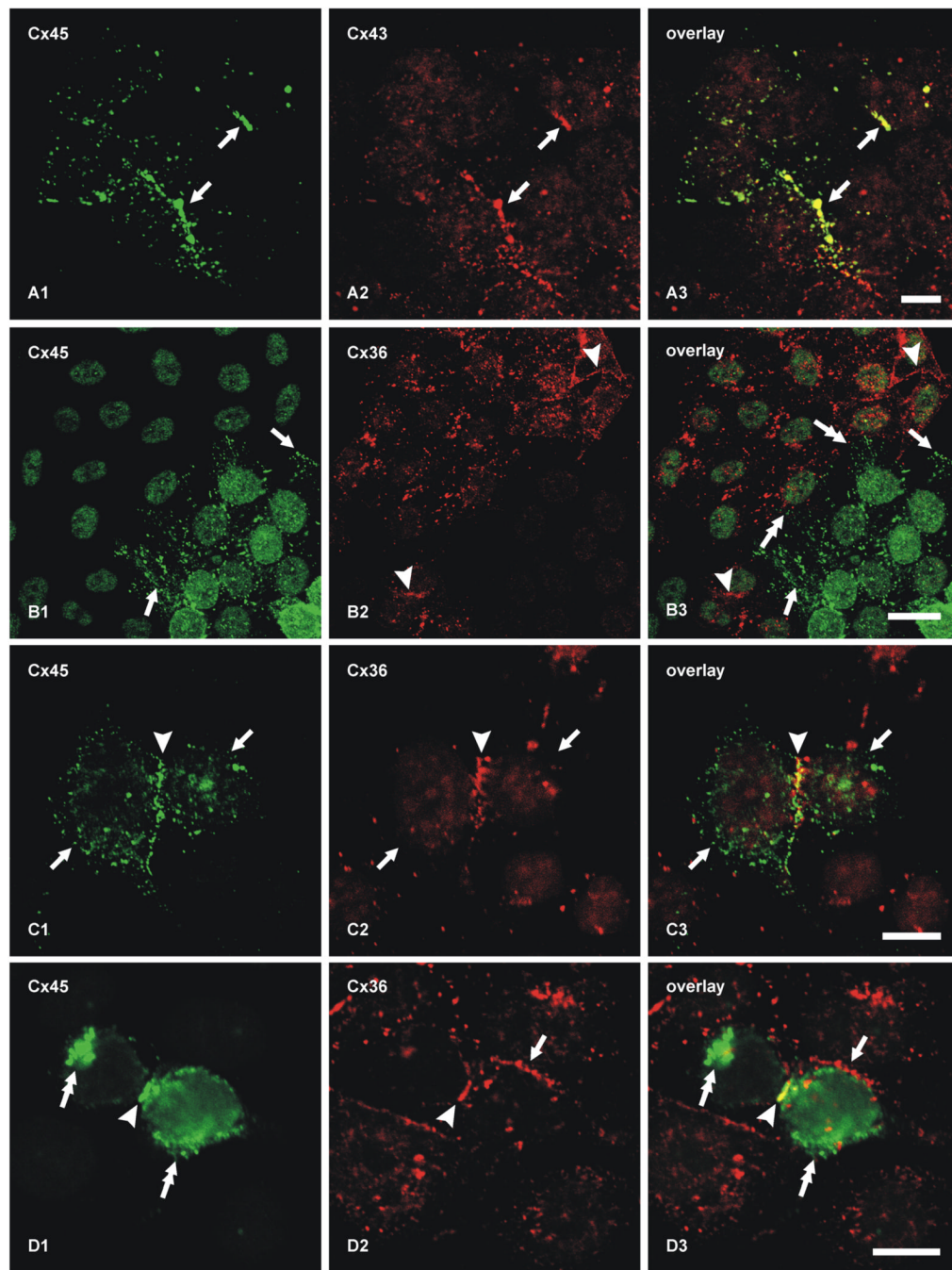


Figure 5.

Double immunofluorescence labeling of connexins in cultures containing mixtures of HeLa cells expressing Cx45, Cx43 or Cx36. **A**, Co-culture of cells stably expressing Cx45 with those expressing Cx43, showing co-localization of Cx45/Cx43 at abutments between Cx45-HeLa and Cx43-HeLa cells (**A1-A3**, arrows, yellow puncta in **A3**). **B**, Co-culture of cells expressing Cx45 with those expressing Cx36, showing Cx45-positive puncta at cell appositions among colonies of Cx45-HeLa cells (**B1**, lower right half of field, and arrows) and Cx36-positive puncta at appositions among Cx36-HeLa cells (**B2**, upper left half of field and arrowheads). There is a lack of Cx45/Cx36 co-localization at abutments between Cx45-HeLa and Cx36 HeLa cells (**B3**, double-headed arrows). **C**, HeLa cells stably expressing Cx36 and transiently

transfected with Cx45, showing two apposed cells (arrows) expressing both connexins, and Cx45/Cx36 co-localization at points of cell-cell contact (arrowhead). **D**, Two HeLa cells stably expressing Cx36 and transiently transfected with Cx45, showing Cx45 localized intracellularly (**DI**, double-headed arrows), Cx36/Cx45 co-localization at points of cell-cell contact between cells expressing both connexins (arrowhead), and absence of Cx45 at points where double-expressing cells make contacts with cells expressing only Cx36 (arrow). Scale bars, 10 μm .

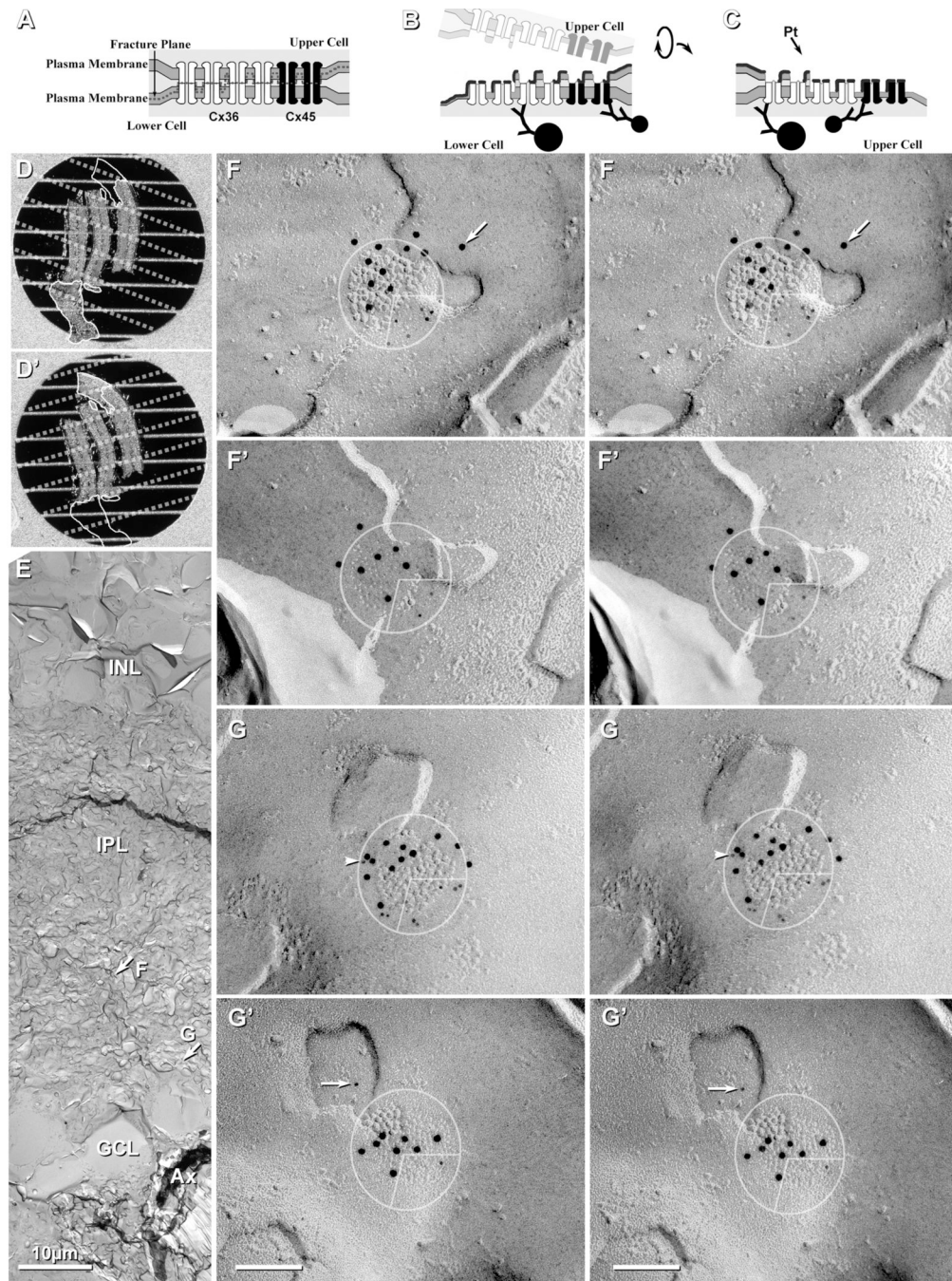


Figure 6. Images and the interpretation of labeling in matched double-replicas. **A-C**, Scale diagram showing gap junction before and after freeze fracturing and retrieval of complementary replicas. **A**, The fracture plane (dashed line) separates connexons at their points of contact in the extracellular space, leaving all connexons of the lower cell for subsequent immunogold labeling. **B-C**, Creation of double-replicas having complementarity of E- and P-fracture faces. Each matching replica contains connexons from only one cell, but the E-face of one cell and the P-face of the other cell. **D, D'**, Images from dissecting microscope showing matched double-replicas containing three strips of retina after SDS washing and immunogold labeling. **E**, Low-magnification image of one side of a complementary replica, with locations of two of the

mapped gap junctions indicated by arrows. *F,F',G,G'*, High magnification stereoscopic views of complementary replicas of two gap junctions, with 10-nm gold labeling Cx36 and 5-nm gold labeling Cx45. Cx36 labeling is present beneath three quadrants of both gap junctions (E-face pits in top replica and complementary P-face particles in bottom replica). 5-nm Cx45 labels are present in the lower right quadrant. Initial pre-coating with 2-3 nm of carbon partially obscured E-face connexon pits. Arrow (in *F*) indicates a gold bead beyond the 28-nm radius of immunogold labeling. Arrowhead (in *G'*) indicates a 5-nm gold label for Cx45, with possible corresponding label in the complementary image (*G*, arrow). Scale bars, 0.1 μm unless otherwise indicated.

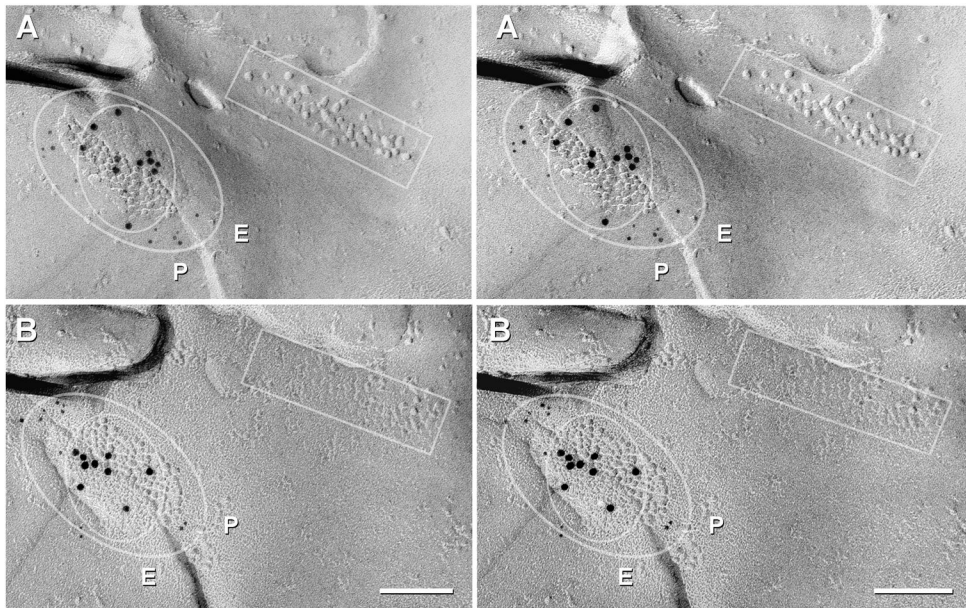


Figure 7.

Cx45/Cx36 double-labeled gap junction adjacent to a ribbon of E-face particles / P-face pits (rectangles) that are found postsynaptic to ribbon synapses, which in IPL, are characteristic of rod and cone bipolar cells. Outer oval delineates the area with increased Cx45 labeling (12 and 11 5-nm gold beads, **A** vs. **B**), and the inner oval delineates the domain of Cx36 labeling (11 and nine 10-nm gold beads, **A** vs. **B**). P, P-face; E, E-face. Scale bars, 0.1 μm

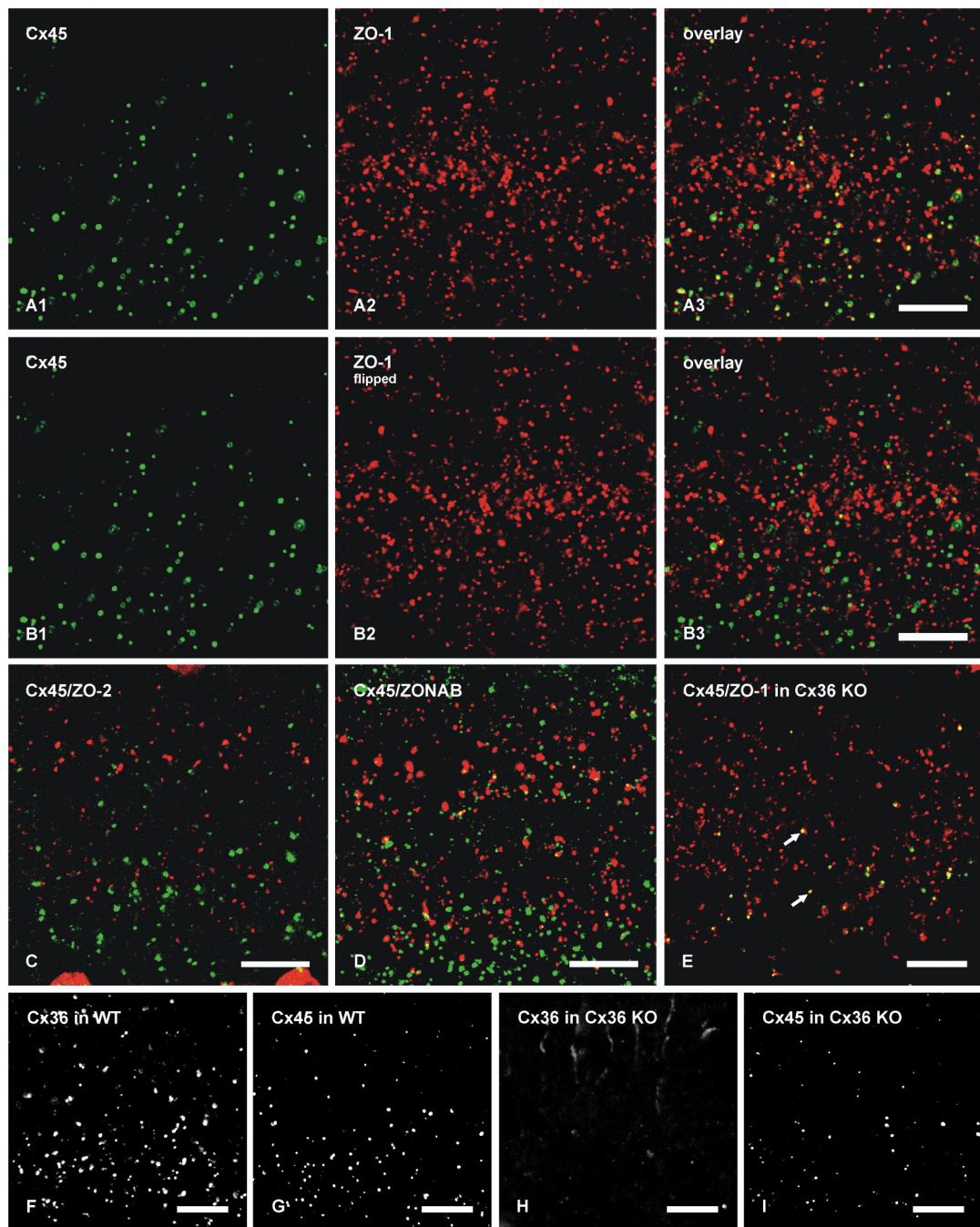


Figure 8.

Laser scanning confocal double immunofluorescence showing relationships of Cx45 with ZO-1, ZO-2 and ZONAB in the IPL of adult mouse retina, and Cx36, Cx45 and ZO-1 in the IPL of adult wild-type and Cx36 ko mice. Images show the IPL from inner (bottom) to outer (top) edge, and represent z-stacks of five confocal scans in **A-D**, and single scans in **E-I**. Co-localization of green and red labeling is seen as yellow in image overlays. **A**, The same field (**A1-A3**) showing a high proportion of Cx45-positive puncta labeled for ZO-1. **B**, The same set of laser scanning confocal double immunofluorescence images as in **A**, showing minimal Cx45/ZO-1 co-localization in the IPL after horizontal flipping of the image showing labeling for ZO-1. **C**, Double immunofluorescence overlay showing lack of Cx45 (green) co-

localization with ZO-2 (red). **D**, Double immunofluorescence overlay showing very few Cx45-positive puncta (green) labeled for ZONAB (red). **E**, Double immunofluorescence overlay showing the persistence of Cx45/ZO-1 co-localization seen as yellow puncta (arrows) in the IPL of Cx36 ko retina. **F-I**, Confocal scans showing Cx36-puncta (**F**) and Cx45-puncta (**G**) in the IPL of wild-type retina, and an absence of labeling for Cx36 (**H**) and a reduction of labeling for Cx45 (**I**) in IPL of Cx36 ko retina. Scale bars, 10 μ m.

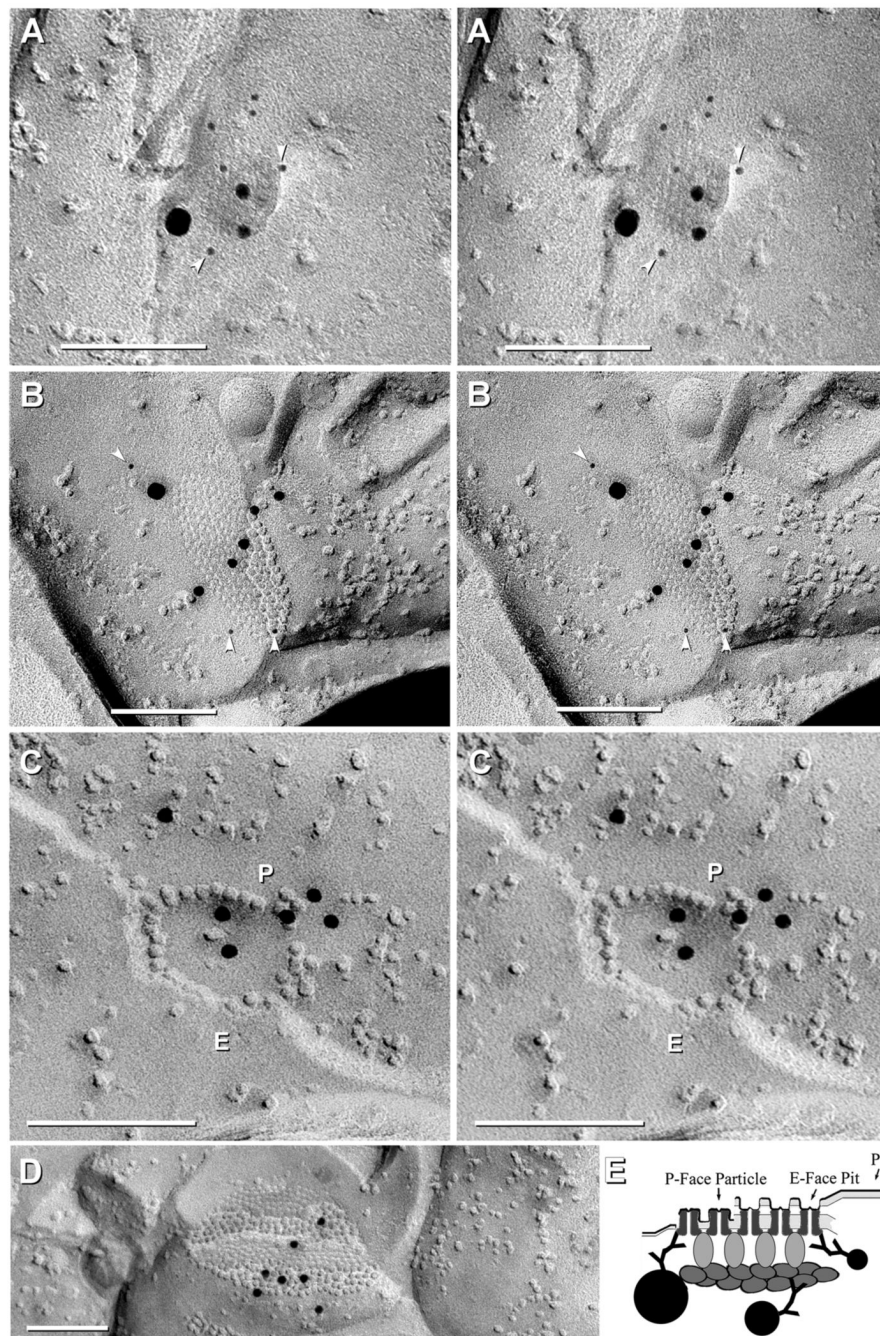


Figure 9.

FRIL images showing co-localization of Cx45 with ZO-1 in rat IPL. **A**, Small crystalline plaque gap junction (41 connexons) double labeled for Cx45 (6-nm gold beads, arrowheads, and one 18-nm gold bead) and for ZO-1 (two 12-nm gold beads). Stereoscopic viewing reveals that the gap junction E-face was almost fractured away, appearing as an attached flake canted above the underlying connexons, similar to that seen in Fig. 6B, above. **B**, Medium-size partially-crystalline plaque gap junction (ca. 154 connexons) double-labeled for ZO-1 (five 12-nm gold beads across the center) and for Cx45 (three 6-nm gold beads, arrowheads, and one 18-nm gold bead, at the periphery). **C**, Small “Q-shaped” string gap junction (ca. 34 connexons, three as E-face pits) labeled for ZO-1 (six 12-nm gold beads) and for Cx45 (6-nm and 18-nm gold

beads; none present). One 12-nm gold bead that is outside the string of connexons may indicate either displacement during washing or the presence of ZO-1 outside the boundary of the gap junction. P = P-face; E = E-face. **D**, Medium plaque gap junction (341 connexons) labeled for ZO-1 (seven 12-nm gold beads, none for Cx45; same replica as A-C). Scale bars, 0.1 μm . **E**, Diagram showing proposed labeling of ZO-1 in the protein scaffolding that comprises the “cytoplasmic semi-dense matrix” (Sotelo and Korn, 1978). The dense matrix of scaffolding proteins may restrict penetration of primary and secondary antibody labels and thereby reduce labeling of connexons in the center of larger plaque gap junction (see Fig. 3E).

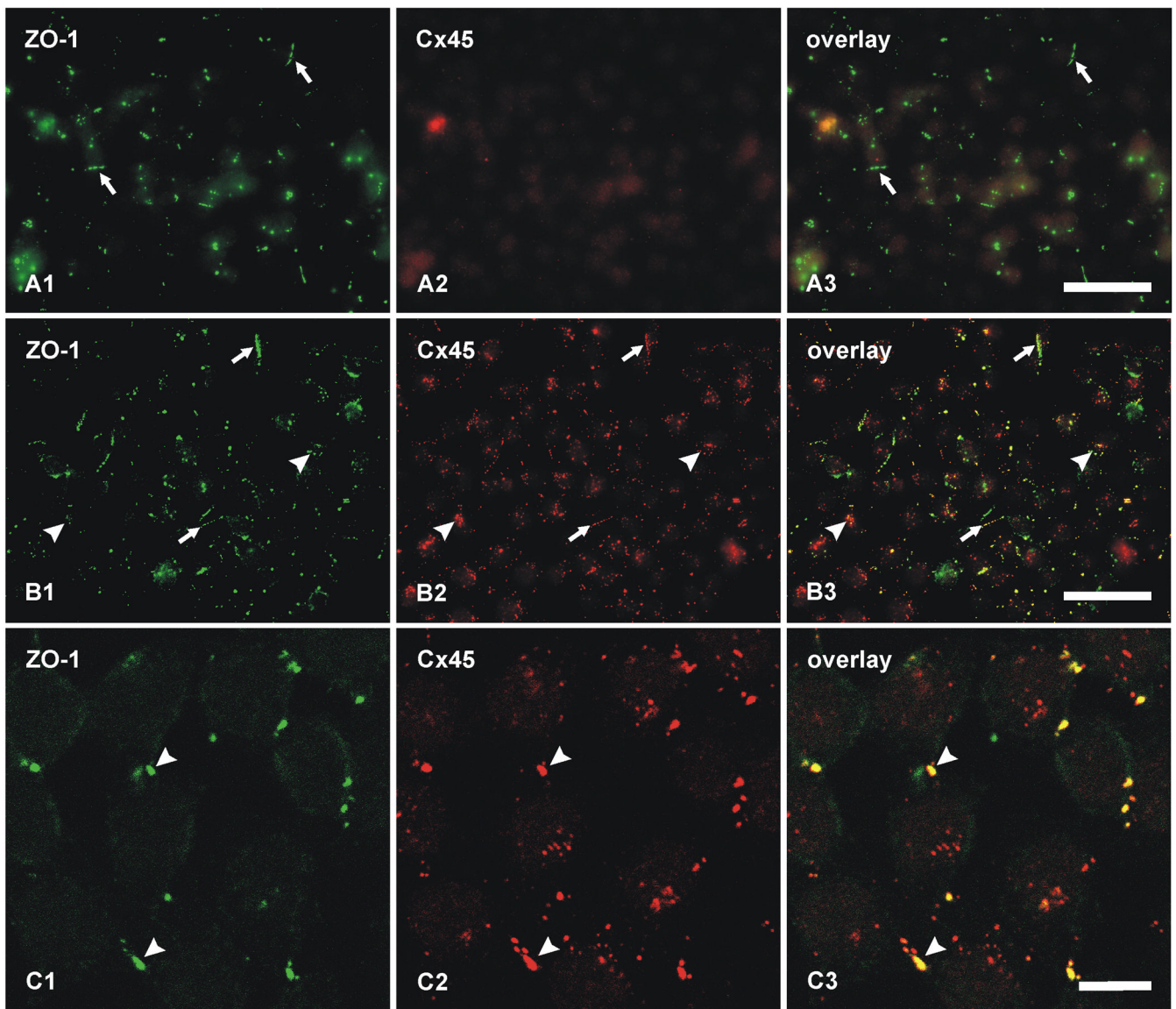


Figure 10.

Double immunofluorescence labeling of ZO-1 and Cx45 in HeLa cell cultures. **A**, Control empty vector-transfected HeLa cells showing labeling of ZO-1 at cell-cell contacts (**A1**, arrows), and an absence of labeling for Cx45 (**A2**). **B**, HeLa cells stably transfected with Cx45. Immunolabeling is seen as linear strands of ZO-1-puncta (**B1**) and Cx45-puncta (**B2**) at cell-cell contacts (arrows), and as collections of puncta within cells (arrowheads). ZO-1/Cx45 co-localization is evident at both locations (**B3**). **C**, Confocal double immunofluorescence showing co-localization of punctate labeling for ZO-1 and Cx45 at contacts between Cx45-transfected HeLa cells (arrowheads). Scale bars, A,B, 50 μm ; C, 10 μm .

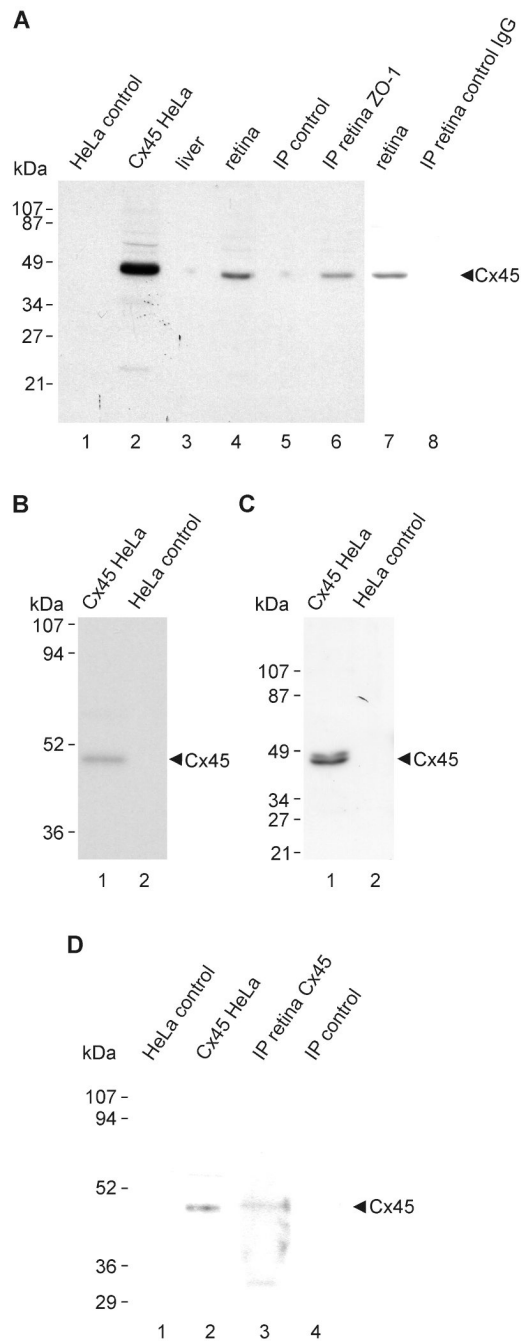


Figure 11.

Immunoblots demonstrating co-IP of Cx45/ZO-1 from retina and detection of Cx45 with polyclonal anti-Cx45. **A**, Cx45 detection by monoclonal anti-Cx45 in lysates of Cx45-transfected HeLa cells (lane 2) and in homogenate of mouse retina (lanes 4 and 7), but not in empty vector-transfected HeLa cells (lane 1) or in liver (lane 3). After IP of ZO-1 from retina homogenate using polyclonal anti-ZO-1, monoclonal anti-Cx45 detects Cx45 (lane 6) comigrating with Cx45 from retina homogenate (lane 4) and from Cx45-transfected HeLa cells (lane 2), but not in IP material after omission of anti-ZO-1 during the IP procedure (lane 5) or after IP of ZO-1 from retina using anti-FLAG as control IgG (lane 8). **B,C**, Polyclonal anti-Cx45 detection of Cx45 as a single band using 12.5% SDS-gel (**B**, lane 1) and as a doublet

of bands using 10% SDS-gel (**C**, lane 1) in lysates of Cx45-transfected HeLa cells, and absence of these bands in empty vector-transfected HeLa cells (**B,C**, lane 2). **D**, IP of Cx45 from retina with monoclonal anti-Cx45, showing detection of a Cx45 band with polyclonal anti-Cx45 in IP material (lane 3), corresponding to a Cx45 band detected by the polyclonal antibody in lysate from Cx45-transfected HeLa cells (lane 2), and absence of the band in empty vector-transfected HeLa controls (lane 1) or after omission of monoclonal anti-Cx45 during the IP procedure (lane 4).

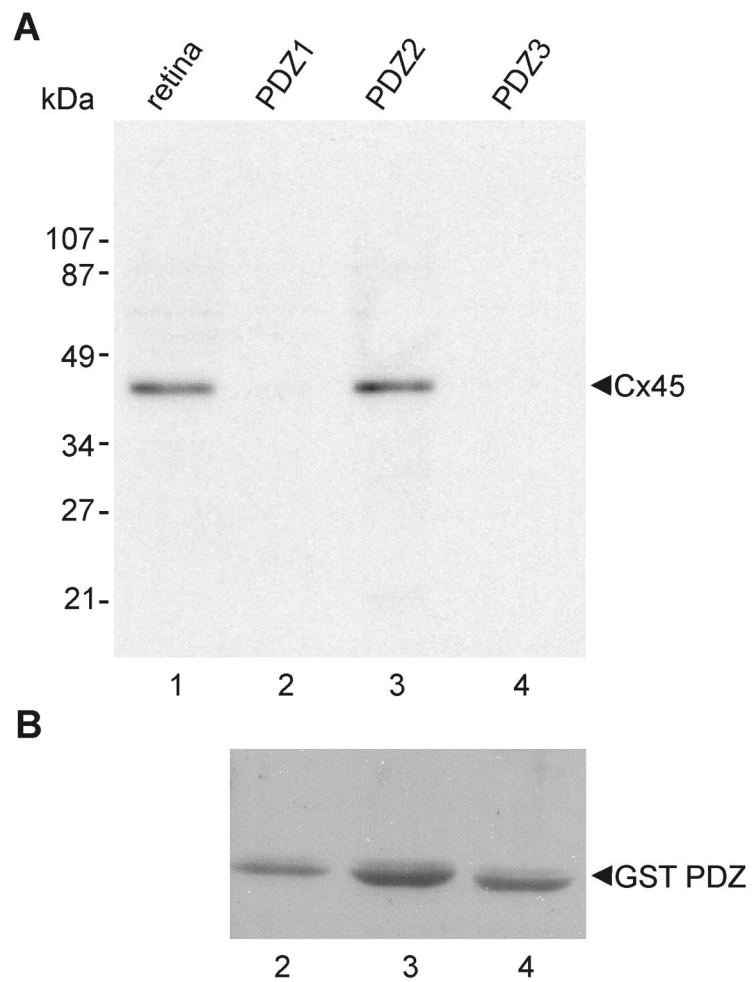
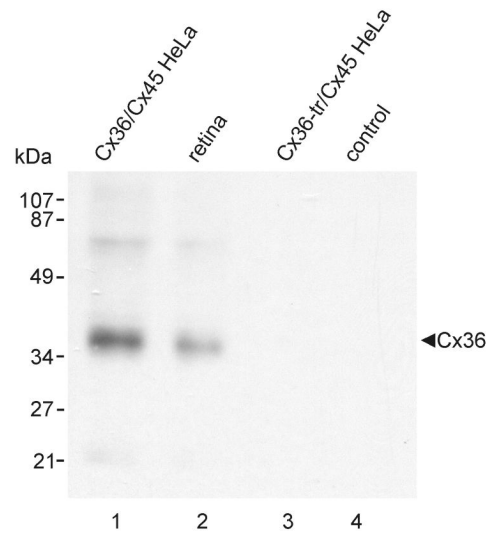
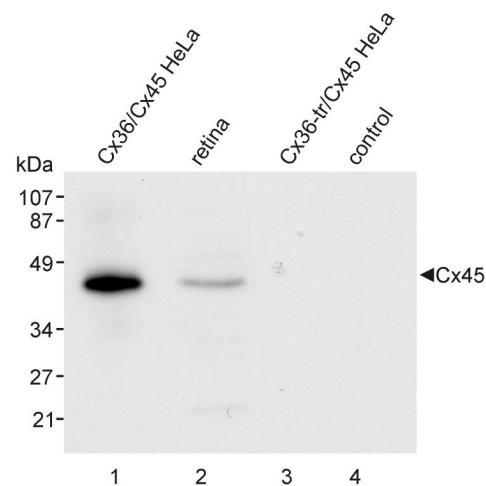


Figure 12.

Immunoblots demonstrating Cx45 pull-down with the PDZ2 domain of ZO-1. Lysates of Cx45-transfected HeLa cells were incubated with GST fusion proteins containing either the PDZ1, PDZ2 or PDZ3 domain of ZO-1. **A**, Immunoblots of pull-down proteins probed with monoclonal anti-Cx45 show detection of Cx45 after pull-down with the PDZ2 domain of ZO-1 (lane 3), but not after pull-down with the PDZ1 or PDZ3 domains of ZO-1 (lane 2 and 4). The Cx45 band in lane 3 corresponds to detection of the same band in homogenate of retina (lane 1). **B**, Blot in **A** was stripped and re-probed with anti-GST antibody to show presence and equal loading of PDZ domain fusion proteins.

A IP of Cx45; probed with anti-Cx36**B** IP of Cx36; probed with anti-Cx45**Figure 13.**

Co-IP of Cx36 with Cx45 from mouse retina and HeLa cells transfected with Cx36 and Cx45.

A, Immunoblot showing detection of Cx36 after IP of Cx45 from mouse retina (lane 2) and from HeLa cells co-transfected with Cx36/Cx45 (lane 1), and absence of Cx36 detection after IP of Cx45 from HeLa cells co-transfected with Cx45 and c-terminus-truncated Cx36 (lane 3) or after IP with omission of anti-Cx45 (lane 4). **B**, Immunoblot showing detection of Cx45 after IP of Cx36 from mouse retina (lane 2) and from HeLa cells co-transfected with Cx36/Cx45 (lane 1), and absence of Cx45 detection after IP of Cx36 from HeLa cells co-transfected with Cx45 and c-terminus-truncated Cx36 (lane 3) or after IP with omission of anti-Cx36 (lane 4).

Table 1
Antibodies used for western blotting and immunohistochemistry

Antibody	Type	Species	Epitope; Designation	Dilution	Source
Cx36	polyclonal	rabbit	c-terminus; 36-4600	1 µg/ml	Invitrogen/Zymed
Cx36	polyclonal	rabbit	mid-region; 51-6300	4 µg/ml	Invitrogen/Zymed
Cx36	monoclonal	mouse	mid-region; 37-4600	3 µg/ml	Invitrogen/Zymed
Cx36	monoclonal	mouse	c-terminus; 39-4200	4 µg/ml	Invitrogen/Zymed
Cx43	polyclonal	rabbit	c-terminus; 71-0700	2 µg/ml	Invitrogen/Zymed
Cx45	polyclonal	rabbit	c-terminus; 40-7000	2 µg/ml	Invitrogen/Zymed
Cx45	monoclonal	mouse	c-terminus; 41-1700	2 µg/ml	Invitrogen/Zymed
Cx45	monoclonal	mouse	aa 354-367; Mab3101	4 µg/ml	Millipore/Chemicon
ZO-1	polyclonal	rabbit	aa 463-1109; 61-7300	1 µg/ml	Invitrogen/Zymed
ZO-1	monoclonal	mouse	aa 334-634; 33-9100	4 µg/ml	Invitrogen/Zymed
ZO-2	monoclonal	mouse	aa 87-208; Ab611561	3 µg/ml	BD Biosciences
ZONAB	polyclonal	rabbit	c-terminus; 40-2800	2 µg/ml	Invitrogen/Zymed
GST	polyclonal	rabbit	whole protein; Ab06-332	1 µg/ml	Millipore/UpState

aa, amino acids

Table 2

Quantitative immunofluorescence analysis of Cx45 co-localization relationships with Cx36, ZO-1, ZO-2 and ZONAB in the IPL of adult mouse retina

Proteins examined	Protein (total puncta counted) <i>I</i>	Percent co-localization ²
Cx45 positive for Cx36 ³	Cx45 (766)	46 ± 7.2
Cx45 positive for Cx36 ⁴	Cx45 (2952)	87 ± 1.3
Cx45 positive for ZO-1	Cx45 (737)	71 ± 2.8
Cx45 positive for ZO-2	Cx45 (432)	7.0 ± 2.1
Cx45 positive for ZONAB	Cx45 (472)	4.7 ± 0.4

¹ Values in parentheses represent the total number of Cx45-positive or Cx36-positive puncta counted in four to ten separate single scan confocal images of the IPL in retinas from two to four mice.

² Values represent means ± SEM.

³ Data from mice prepared with 40 ml of fixative, with immediate washout.

⁴ Data from mice prepared with 20 ml of fixative, with immediate washout.

Table 3

Numbers of gap junctions labeled for Cx36, Cx45, or Cx36+Cx45 in FRIL single-replicas of mouse and rat retinas that were double-labeled for Cx36 plus Cx45.

Antibody	Mouse		Rat	Total
	Shorter Labeling ¹	Longer Labeling ²	Shorter Labeling	
Cx36	408 (92%)	137 (88%)	62 (85%)	607 (90%)
Cx36 + Cx45	29 (7%)	19 (12%)	10 (14%)	58 (9%)
Cx45	5 (1%)	0 (0%)	1 (1%)	6 (1%)
Total	442 (100%)	156 (100%)	73 (100%)	671 (100%)

¹ Shorter labeling was defined as 1–4.4 h for primary and 12–17 h for secondary antibody labeling; no significant differences were noted between 1–1.2 h and 4.4 h for primary antibodies.

² Longer labeling was defined as 5.3–6.8 h for primary and 21.5 h for secondary antibodies.

Numbers in parentheses indicate percentage of labeled gap junctions found in each labeling protocol. These data do not include the 160-plus Cx36 and Cx36+Cx45-containing gap junctions found in the double replicas (see Table 4).

These data do not include the 160-plus Cx36 and Cx36+Cx45-containing gap junctions found in the double-replicas (See Table 4).

Table 4

Numbers of gap junctions in single and double replicas, per cent of Cx45+Cx36 double-labeled gap junctions, and lower and upper confidence intervals (CI) at 95% confidence levels for Cx45-containing gap junctions expressing both connexins.

Observed	Percent	Lower 95% CI	Upper 95% CI
19/19 ¹	100.00%	85.4%	100.0%
41/45 ²	91.1%	78.8%	97.0%
60/64 ³	93.8%	84.8%	98.3%
20/22 ⁴	90.9%	70.8%	98.9%
8/10 ⁵	80%	44.4%	97.5%

¹ Cx45+Cx36-containing gap junctions from three FRIL replicas that were labeled for longer times in both primary and secondary antibodies.

² Cx45+Cx36-containing gap junctions from the other 15 FRIL replicas.

³ Cx45+Cx36-containing gap junctions, data combined from all 18 FRIL replicas.

⁴ Cx45+Cx36-containing gap junctions from 11 paired and 1 unpaired hemiplaques, calculated as individual hemiplaques, from one SDS-FRL double-replica.

⁵ Cx45+Cx36-containing gap junctions from paired matched hemiplaques, calculated as pairs, from one SDS-FRL double-replica. (Not included is the pair with label for Cx45 and Cx36 on one side and neither label on the other side.)